12

David Taylor Research Center
Bethesda, MD 20084–5000

DTRC–SME–90/74 October 1990
Ship Materials Engineering Department
Research and Development Report

A Comparison of the Compression Response of Thick (6.35 mm) and Thin (1.60 mm) Dry and Moisture Saturated AS4/3501–6 Laminates

by
Karin Gipple

Dry and Moisture Saturated AS4/3501–6 Laminates

MAJOR DTRC TECHNICAL COMPONENTS

CODE 011 DIRECTOR OF TECHNOLOGY, PLANS AND ASSESSMENT

12 SHIP SYSTEMS INTEGRATION DEPARTMENT

14 SHIP ELECTROMAGNETIC SIGNATURES DEPARTMENT

15 SHIP HYDROMECHANICS DEPARTMENT

16 AVIATION DEPARTMENT

17 SHIP STRUCTURES AND PROTECTION DEPARTMENT

18 COMPUTATION, MATHEMATICS & LOGISTICS DEPARTMENT

19 SHIP ACOUSTICS DEPARTMENT

27 PROPULSION AND AUXILIARY SYSTEMS DEPARTMENT

28 SHIP MATERIALS ENGINEERING DEPARTMENT

DTRC ISSUES THREE TYPES OF REPORTS:

1. **DTRC reports, a formal series,** contain information of permanent technical value. They carry a consecutive numerical identification regardless of their classification or the originating department.

2. **Departmental reports, a semiformal series,** contain information of a preliminary, temporary, or proprietary nature or of limited interest or significance. They carry a departmental alphanumerical identification.

3. **Technical memoranda, an informal series,** contain technical documentation of limited use and interest. They are primarily working papers intended for internal use. They carry an identifying number which indicates their type and the numerical code of the originating department. Any distribution outside DTRC must be approved by the head of the originating department on a case-by-case basis.

NDW-DTNSRDC 5602/51 (Rev 2-88)

David Taylor Research Center
Bethesda, MD 20084–5000

DTRC–SME–90/74 October 1990
Ship Materials Engineering Department

A Comparison of the Compression Response of Thick (6.35 mm) and Thin (1.60 mm) Dry and Moisture Saturated AS4/3501–6 Laminates

by
Karin Gipple

TABLE OF CONTENTS

LIST OF TABLES

LIST OF FIGURES

ADMINISTRATIVE INFORMATION

This project was partially sponsored by the Office of Naval Research (ONR), and administered by the David Taylor Research Center (DTRC) Materials Block Manager, Mr. Ivan Caplan (Code 0115) under Program Element 62234N, Task Area R3450SOS and DTRC Work Unit 1-2802-950.

Additional support was provided by the DTRC Internal Research (IR) program sponsored by the Space and Naval Warfare Systems Command Director of Navy Laboratories, SPAWAR 05, and administered by Dr. Bruce Douglas (Code 0112) under Program Element 61152N, Task Area R000N00 and DTRC Work Unit 2844-220.

ABSTRACT

The compression response of thick (6.35 mm) and thin (1.60 mm) $(0_2/90)_s$ AS4/3501-6 laminates was compared for material in the dry and moisture saturated conditions. The thick specimens failed at 1055 MPa dry and 740 MPa wet. Comparable strengths for the thin specimens were 1090 MPa and 957 MPa. There was no statistical difference in strength for the dry material of either thickness. The thick specimens absorbed significantly more water than the thin specimens, and consequently, showed a greater loss in compression strength.

The elastic modulus was not affected by moisture in the thick or thin specimens.

The gross failure mode of the dry and wet specimens of either thickness was very similar with slightly more delamination occurring in the wet specimens. The thick specimens typically exhibited angular cracks of 27° to 30° partially across the specimen thickness. This was not observed in the thin specimens.

Finite element techniques were used to determine shear stresses in the matrix for a fiber-matrix composite plate with an initial imperfection, and loaded in compression. These matrix shear stresses were used

in a compression failure theory which showed reasonable agreement with experimental results. It appears that the detrimental influence of the moisture is the degradation of the matrix shear modulus at high compressive stresses with high moisture concentrations.

BACKGROUND

INTRODUCTION

Fiber reinforced composite materials have become increasingly popular, in part, due to their high strength to weight ratios and the ability to orient the reinforcement in the principal stress directions. The primary applications of such materials have been in the aircraft and sporting industries with typical products usually involving thin sections with tensile loadings. New applications for these materials are currently being explored for naval and biomedical hardware where the products involve thicker sections loaded in compression while exposed to a moist environment.

The usefulness of the composite materials database as it currently exists for these new applications is unclear because studies conducted over the past twenty years have focused primarily on the behavior of thin sections loaded in tension. Composite materials often do not exhibit the same behavior in compression as in tension [1,2]. Differences in elastic moduli, strengths and failure modes have been observed. Fabrication quality also becomes more important if the component is to be loaded in compression. Compressive strengths are very sensitive to composite void contents and initial fiber waviness [3,4,5,6,7], and void contents of less than 1% to 2% are required to

avoid significant reductions in compression strength [8].

Current compression test methods for composites have been developed for thin sections based on the requirements of the aircraft industry. These methods transfer the load by shear from the grips to the specimen. Characterization of the compression response of thick section composites using these methods is unlikely. The very large loads required for failure of the thick sections eliminate the option of transferring the load by shear from the grips to the specimen. New test methods may have to be developed to assess the effect of thickness on compression behavior [9].

Environmental conditioning introduces additional complications. The typical conditioning procedure used by the aircraft industry requires full saturation of the specimen in a hot, humid environment [10,11,12]. However, this procedure may be unrealistic for thick sections with applications in environments that require total immersion in seawater at or near room temperature. Full saturation of thick sections at these low temperatures is not feasible due to the extremely long period of time required for saturation.

Fabrication, environmental conditioning and compression testing of specimens with thin sections is easier and less expensive than comparable procedures for thick laminates. Nevertheless, if significant differences

are observed between the mode of failure for thin and thick specimens, then it is clear that thin specimens cannot be used to characterize properties of thick section laminates.

The first objective of this study is to address these issues by examining the changes in the failure mode and/or strength between thin 1.6 mm (0.0625 in.) and thick 6.35 mm (0.25 in.) graphite/epoxy laminates loaded in uniaxial compression. The second objective is to compare the fracture behavior for both dry and "wet" (moisture conditioned) specimens.

LITERATURE REVIEW

COMPRESSION TESTING OF COMPOSITE MATERIALS

Compression testing of composite materials usually follows the procedures outlined in ASTM D3410-87 [13]. Two fixtures recommended in this standard are the Celanese and IITRI (Illinois Institute of Technology Research Institute) compression test fixtures [14,15]. These two fixtures are illustrated in Figures 1 and 2. With both fixtures, the compressive load is transmitted by shear from the wedged grips to the specimen. The IITRI fixture differs from the Celanese primarily in the design of the wedged grips [13]. Trapezoidal wedges are used in the IITRI fixture which maintain surface contact between the grips and the alignment blocks for specimens with tabbed end thicknesses of 1.5 mm (0.06 in.) to 12.7 mm (0.50 in.) [14]. The conically shaped wedges of the Celanese fixture limit the tabbed end thickness to a maximum of 4.06 mm (0.16 in.) because greater thicknesses cause a line instead of a surface contact between the conical wedge and tapered collet [14].

Recommended specimen geometries for either fixture are also given in ASTM D3410-87, and these dimensions depend upon the material being tested. For example, the thicknesses of a unidirectional laminate of graphite/epoxy should range between 1.5 to 3.0 mm (0.06 to 0.120 in.).

Specimen widths and gage lengths are specified at 6.35 mm (0.25 in.) and 12.70 mm (0.50 in.), respectively. Tabs are required for all specimens and should be 63.5 mm (2.50 in.) long and 6.35 mm (0.25 in.) wide with a 6.35 mm (0.25 in.) taper toward the specimen gage area. Design and precision in machining the specimen used with this test method is critical. To minimize bending strains due to specimen eccentricity requires that the tab surfaces be ground flat and parallel to within 0.05 mm (0.002 in.) [16]. In addition, the specimen gage lengths recommended in ASTM D3410 must be reviewed for new composite materials with varying degrees of anisotropy. The gage length must be long enough to accomodate the stress concentration effects introduced at the tab ends, but short enough to avoid Euler buckling. The specimen length necessary to attenuate stress concentrations due to the specimen ends and/or grips for anisotropic materials can exceed several specimen thicknesses [17].

Composite materials have also been tested in compression using the sandwich beam specimen shown in Figure 3 [18]. This specimen consists of two skins of composite material bonded to a honeycomb core. The skin that is exposed to compression when bending loads are applied to the specimen is made thinner than the tension skin to force failures in the compression layer.

Each of the preceding methods have disadvantages. The

requirement for specimen tabs significantly complicates specimen preparation for the IITRI/Celanese methods. In addition, testing of high strength materials or thicker cross-section specimens is limited by the shear strengths of available adhesives which are used to bond the tabs to the specimens [14]. Typical adhesive shear strengths range from 35 to 42 MPa (5 to 6 ksi) limiting compressive loads to 33.4 kN (7500 lbs.) for a 63.5 mm (2.50 in.) by 6.35 mm (0.25 in.) attachment area [19]. The specimen length required for the attenuation of stress concentrations due to the specimen ends and/or grips also increases with thickness [17]. This requirement complicates specimen design as analyses have to be performed for each specimen thickness to determine the appropriate decay length. Finally, the sandwich beam specimen is applicable only to very thin laminates 1.020 mm (0.040 in.), and requires a large amount of composite material for fabrication [14, 18].

Loading of composites in compression directly through the specimen ends is advantageous as the requirement for end tabs and limits on cross-sectional areas are eliminated. Another standard, ASTM D695, a compression test for rigid plastics, recommends loading the ends of a "dogbone" shaped specimen which is bolted in a fixture that supports the specimen length. This fixture and specimen are shown in Figures 4 and 5 [20]. The specimen

configuration is only for materials with thicknesses of 3.2 mm (0.125 in.) or less, and has not been found acceptable for the high modulus fiber reinforced composite materials considered in this investigation [15]. Examples of compression fixtures for thicker specimens are also provided as guidelines in this test standard. To date, fixtures which apply loads through the specimen ends appear to be independently developed [9,14,21,22]. A distinguishing feature of these designs is that some type of lateral support is usually required to prevent end brooming, particularly in unidirectional laminates [14]. For example, Barker and Balasundaram [21] developed a fixture consisting of two steel clamping blocks which supported all four sides of the specimen ends over a length of 40 mm (1.57 in.). The specimen ends were ground flat and parallel, and the compression load was applied directly to these ends. In using this fixture, they observed that approximately 20% of the total load had to be transmitted by shear forces developed by the steel blocks. If all the load was transmitted through the ends, premature failures occurred within the clamping blocks. If the shear forces exceeded 20% of the load, premature failures occurred at the edge of the clamp.

A similar fixture was designed by Camponeschi [9] at the David Taylor Research Center. Two steel clamping blocks support the specimen at each end as illustrated in

Figure 6. The bolt torque required to prevent end brooming due to Poisson effects is dependent on the specimen thickness, and must be calculated. Also, tabs were adhesively bonded to each specimen over the clamping area.

Comparisons of test results obtained using the three preceding test methods, IITRI/Celanese, sandwich, and end loading, show that the longitudinal elastic modulus is independent of the compression test method used [14,15]. The results for compressive strength determined with the IITRI/Celanese and sandwich beam methods are comparable if the specimens are thin and properly prepared [15]. Some difficulties have been reported using the Celanese method where slippage occurred between the grips and the tabs on graphite/epoxy specimens. However, slippage was not observed with the IITRI fixture. The problem was attributed to the shallow serrations of the Celanese fixture as compared to the coarser serrations found in the IITRI grips [14].

Variations in the compression strength and the failure mode obtained with the IITRI fixture have been noted with changes in the gage length to thickness ratio [23]. Smoot reported that the highest compressive strengths for unidirectional graphite/epoxy occurred with a length to thickness ratio of 8.7. The failure mode corresponding to that strength was at a transition between angular shear

across the specimen width and brooming within the gage section. Schematics of these failure modes are shown in Figure 7 [23]. Exceeding a length to thickness ratio of 8.7 resulted in a rapid decrease in failure strength, triggered by specimen Euler buckling. Strengths also dropped, but less rapidly, if a length to thickness ratio less than 8 was used. It should be noted that the ASTM Standard D3410 recomends a length to thickness ratio in the range of 4.2 to 8.3.

Test methods using end loading have met with limited success. Lower strengths for unidirectional laminates have been reported using these methods as compared to the other compressive test methods [9,15,22]. The lower strengths were attributed to premature failures by end brooming. This type of failure may be due to Poisson effects, or to stress concentrations caused by uneven fiber ends or transverse friction loads on the ends of the specimen [14,15]. However, Barker and Balasundaram, using the end loading fixture previously described, obtained compressive strengths of 1470 MPa (210 ksi) for unidirectional graphite/epoxy. This correlates very well with strengths obtained by the other methods [15,23].

The use of end loading techniques with cross ply or angle ply laminates has been more successful [9,22]. Strengths of unidirectional laminates of graphite/epoxy estimated from cross ply compression test results (6.35 mm

thick specimens) using Camponeschi's fixture agreed well with those determined using the IITRI/Celanese methods [9]. These more satisfactory results may be due to the transverse support provided by the 90^{o} reinforcement in the cross ply laminate [24]. However, as the specimen thicknesses were increased from 6.35 mm (0.25 in.) to 25.4 mm (1.00 in.), the cross ply laminate strengths dropped by 21%. Since laminates of these thicknesses have rarely been tested, it is not possible to conclude if the loss of strength is due to material changes, or to the test method.

Pressure cylinders fabricated with composite materials with wall thicknesses exceeding 12.7 mm (0.50 in.) provide one source of comparison. The wall stresses in thick walled graphite/epoxy cylinders at failure were significantly below typical flat laminate strengths [9 25]. This trend was not observed in fiberglass reinforced cylinders [26,27].

For a more complete review of compression test methods for composite materials, the reader is referred to Reference 28.

COMPRESSION FAILURE THEORIES

Since the 1960's, numerous researchers have attempted to analytically describe and quantify the failure of composite materials under compressive loads. Development of compression failure theories has been difficult due to the multiplicity of failure modes seen with variations in constituent properties and laminate construction [1]. If these failure theories are grouped according to the particular failure mode addressed, three general categories of failure theories emerge -- fiber microbuckling, kink band formation, and combined failure modes. A brief characterization of typical compression failure theories from each of the three categories is given below.

Historically, the failure mode most frequently applied to unidirectional composites subjected to compressive stress is that of fiber microbuckling. Rosen [29] proposed one of the earliest theories based on fiber microbuckling where the fibers and matrix were modeled as Timoshenko columns supported by an elastic foundation. Expressions for the compression strength were derived for both the extensional and shear buckling modes. In the extensional mode, the fibers buckle out of phase, and in the shear mode, they buckle in phase. Equation (1) shows Rosen's expression for the shear mode of failure in compression, which was the mode most commonly observed in

unidirectional composites.

$$\sigma_c = G_{LT} \quad (1)$$

σ_c= compression strength
G_{LT}= inplane shear modulus of composite

Compression strength values obtained with this theoretical expression significantly overpredicted experimental results.

Additional fiber microbuckling theories including three dimensional models, initial ply waviness and material nonlinearities were developed in an attempt to improve correlations between theory and experimental observations [30,31,32]. Using a 3-dimensional model and energy methods, Greszczuk derived two expressions for the microbuckling stress of a composite based on the fixity of the fiber ends.

$$\sigma_c = G_{LT} + \left(\frac{\pi^2 E_f V_f}{4}\right)\left(\frac{r}{l}\right)^2 \text{ Simply supported} \quad (2)$$

$$\sigma_c = G_{LT} + \pi^2 E_f V_f \left(\frac{r}{l}\right)^2 \text{ Fixed} \quad (3)$$

G_{LT}= in-plane shear modulus of composite
E_f= longitudinal modulus of fiber
V_f= fiber volume fraction
r= fiber radius
l= specimen length

It was noted that these expressions do not account for nonlinear matrix behavior or the initial fiber deformations which could significantly affect the

microbuckling loads. Good agreement was demonstrated between this theory and experiments with composites fabricated from low modulus resins. However, for composites with high modulus resins, the theory is not applicable because failure is not due to microbuckling. This fact led to the development of another relation for the compression strength based on a rule of mixtures formulation [30].

$$\sigma_c=\sigma_f V_f+\sigma_r(1-V_f) \tag{4}$$

σ_f= fiber compressive strength

σ_r= matrix compressive stress corresponding to a strain of $\frac{\sigma_f}{E_f}$

The effects of initial fiber waviness and matrix nonlinearities were addressed by Davis who modeled fiber and matrix layers as a multilayered Timoshenko beam [33]. Critical strength expressions for failure by delamination and failure by shear instability were developed and these relations correlated well with experimental results for boron/epoxy laminates. The critical failure load for shear instability was a function of the shear moduli and volume fractions of both the fiber and matrix as shown below.

$$\sigma_C=\frac{G_f G_m}{V_f G_m+V_m G_f} \tag{5}$$

G_f= shear modulus of fiber

G_m= shear modulus of matrix

V_m= matrix volume fraction

However, Davis cautions that the matrix shear modulus used in Equation (5) must correspond to the shear stress-strain state in the matrix, so that the nonlinearity of the shear modulus of the matrix is reflected in the solution. The stress-strain state in the matrix is determined from a finite difference solution for the multilayered Timoshenko beam subjected to an axial load.

Hahn [1] also developed an expression for the critical microbuckling stress of a composite incorporating both initial fiber waviness and matrix nonlinearities.

$$\sigma_c = V_f \frac{G_{LT}}{1+\frac{\pi E_f d_f}{2\sigma_b l}\left(\frac{\pi f_o}{l}\right)} \qquad (6)$$

σ_b= fiber flexural strength

d_f= fiber diameter

$\frac{f_o}{l}$= amplitude to length ratio of initial fiber imperfection

Experimental validation of Equation (6) showed reasonable agreement for composites with resin tensile moduli between 3 and 5 GPa (.429E6 psi and .716E6 psi).

The second group of failure theories which are closely related to fiber microbuckling, focus on the development of kink bands in unidirectional composites under compressive loads (See Figure 8). Hahn [1] found that

fiber microbuckling occurred in composites with low modulus resins, while fiber kinking was the typical failure mode for composites with high modulus resins. Microscopically, fiber microbuckling was characterized by high bending strains and the consequent development of multiple fiber breaks. Hahn defined failure in the kinking mode with two breaks per fiber, where the short broken segments align in a parallel pattern rotated at an angle less than 90^{o} to the applied compressive load. Typical kink band angles for graphite/epoxy ranged from 22^{o} to 26^{o}. No attempt was made to develop a theoretical expression for the compression strengths based on the kink band failure mode.

Kink band formation under compressive load was also described by Budiansky [34], and incorporated the effects of matrix plasticity and initial fiber waviness. The compression strength based on this theory was a function of the kink band angle, the effective transverse shear modulus of the composite and the transverse Young's modulus as shown in Equation (7).

$$\sigma_c = \left[\frac{\gamma_Y}{\pi+\gamma_Y}\right](G_{LT}+E_T\tan\beta) \qquad (7)$$

γ_Y= strain corresponding to shear yield stress
π= initial imperfection
G_{LT}= inplane shear modulus of composite
E_T= transverse modulus of composite
β= kink band angle

From the preceding discussion, it is clear that a single expression for the compression strength of a composite does not predict the multiple failure modes observed under compressive loads. This fact led a number of researchers to develop multiple mode failure theories. Sinclair and Chamis [35] developed four expressions for compressive strengths each linked to a different failure mode. Their models addressed fiber microbuckling, delamination, bending, and compression failure of the fibers. A similar approach was used by Piggott [36] who derived six different failure models.

More recently, Shuart [37] developed a method considering three mechanisms leading to failure under compressive loads. These included matrix compression, interlaminar shearing due to out of plane waviness in the ply, and inplane matrix shearing which was affected by inplane fiber waviness and fiber scissoring. The uniqueness of Shuart's approach is that it addressed compression failures in both unidirectional and angle ply laminates. The composite laminate was modeled as a series of Kirchhoff plates and elastic foundations with initial out of plane imperfections having the same shape as the critical short wavelength buckling mode. Nonlinear equilibrium equations for the laminate were derived using von Karman nonlinear strain-displacement relations and the principle of stationary potential energy. Solution of

these equations assuming linear elastic material properties yielded displacements, strains, and stresses.

Experimental investigations conducted by Shuart showed that one failure mechanism predominated for a particular range of angles in the angle ply laminates. For example, interlaminar shearing was the dominant failure mode when the longitudinal axes of the plies were oriented from 0^{o} to 15^{o} from the loading axis. Theoretical predictions of failure mode and strength generally correlated well (within 5%) with experimental observations for laminates with plies oriented between 45^{o} and 90^{o}. However, for unidirectional laminates, the failure strengths predicted were significantly less than the experimentally determined strengths.

The compression failure theory of Davis [6] was chosen for this study to compare the difference in compression strengths between wet and dry specimens for several reasons. First, is that the author demonstrated good agreement between theory and experiment for unidirectional boron/epoxy laminates which failed by shear instability (as defined in Reference [6]). This is important because the response of the $(0_2/90)_s$ laminates in this study will be dominated by the 0^{0} plies, and shear instability has been an observed failure mode for these laminates in previous studies [9,23]. Shuart [22] also predicted interlaminar shearing as a failure mode for

unidirectional laminates, but his predicted compression strengths were significantly lower than those commonly observed for unidirectional AS4/3501-6 laminates.

Secondly, the form of the failure theory, as shown in Equation (5), is representative of many of the microbuckling based theories and Budiansky's [34] kink band theory. For example, if the shear modulus (G_{LT}) of a multilayer beam is derived by considering the shear modulus of each layer as springs in parallel, then Equation (5) states that the compression strength of a composite is equivalent to its shear modulus. This conclusion is the same as Rosen's [29], and a lower bound for Greszczuk's [30] microbuckling theories.

And lastly, since the shear modulus of a composite is highly nonlinear, some methodology must be proposed to choose a modulus for use in the failure theory. Davis [6] recommended such an approach including the effects of nonlinear matrix behavior and fiber waviness. Davis based his approach on Timoshenko beam theory and solved the resultant equations with finite difference techniques, but other numerical techniques such as finite element methods would be equally applicable to this problem.

DIFFUSION BEHAVIOR IN COMPOSITE MATERIALS

Understanding the effects of moisture on composite mechanical behavior requires the ability to estimate the amount of water a composite will absorb under a specified set of environmental conditions. Most of the data currently available regarding composite materials and moisture absorption has been generated by the aircraft industry. Graphite/epoxy is the material most frequently cited, and the environmental exposure is typically hot and humid [10,11,38]. Specimens are usually exposed to this environment until full saturation occurs which is manifested by no further increases in specimen weight with continuing exposure [38]. Much less information is available on the effects of immersion as compared to humidity conditioning, and moisture gradients through the thickness as compared to a constant moisture concentration. These issues are pertinent to new applications for composite materials. Moisture diffusion in composites is further complicated by the number of parameters that can affect the process, which include void content, fiber orientation, stress state, resin material, and degree of cure [39,40]. If it is assumed that the fiber is impervious, all the moisture absorbed by a composite is attributed to the resin material [41]. The rate of diffusion of water into a polymer material is then modeled by Fick's Law [42]:

$$\frac{\partial C}{\partial t}=D\frac{\partial^2 C}{\partial z^2} \tag{8}$$

C=moisture concentration
D=diffusion coefficient through thickness
z=thickness coordinate

The solution of this partial differential equation for a system with an initial uniform moisture concentration of C_o, and moisture concentrations of C_1 and C_2 at the -h/2 and +h/2 (see Figure 9) surfaces respectively is [43,44]:

$$C(z,t)=C_1+(C_2-C_1)\frac{z}{h}+\frac{2}{\pi}\sum_{n=1}^{\infty}\frac{C_2\cos(n\pi)-C_1}{n}\sin(\frac{n\pi z}{h})e^{\frac{-Dt}{h^2}n^2\pi^2}$$

$$+\frac{4C_0}{\pi}\sum_{m=0}^{\infty}\frac{1}{2m+1}\sin\frac{(2m+1)\pi z}{h}e^{\frac{-Dt}{h^2}(2m+1)^2\pi^2} \tag{9}$$

For experimental purposes, it is helpful to calculate M, the per cent weight gain.

$$M=\frac{W_W-W_D}{W_D} \tag{10}$$

W_W= weight of wet material
W_D= weight of dry material

which can also be expressed as [38]

$$M=G\int_{\frac{-h}{2}}^{\frac{h}{2}}C\partial z \tag{11}$$

G= time dependent parameter
defined below

The integration of Equation 11 gives [45]

$$G = \frac{M-M_i}{M_m-M_i} = 1-\frac{8}{\pi^2}\sum_{j=0}^{\infty}\frac{e^{-(2j+1)^2\pi^2(\frac{Dt}{h^2})}}{(2j+1)^2} \qquad (12)$$

M_i=initial moisture content

M_m=maximum moisture content

D=diffusion coefficient through the thickness

t=time

h=thickness

Springer [38] approximates this solution for a material exposed to moisture on two sides by

$$G=1-\exp[-7.3(\frac{Dt}{h^2})^{.75}] \qquad (13)$$

A composite material formed of water absorbing resin and an impervious fiber will absorb less moisture than the pure resin. The diffusion coefficient of moisture through the thickness will be a function of fiber angle and fiber volume fraction. An expression for this coefficient has been developed by Shen and Springer [38]

$$D=D_{11}\cos^2\alpha+D_{22}\sin^2\alpha \qquad (14)$$

$D_{11}=D_r(1-V_f)$

$D_{22}=D_r(1-2\sqrt{\frac{V_f}{\pi}})$

D_{11}=diffusivity parallel to fibers

D_{22}=diffusivity perpendicular to fibers

D_r=resin diffusion coefficient

α=orientation of fibers with respect to z axis, 90° (See Figure 10)

V_f= fiber volume fraction

If a composite specimen is exposed to moisture without coating its edges, correction for the edge effects must be incorporated into the calculation of the diffusion coefficient. For a unidirectional composite oriented as shown in Figure 10:

$$D_z=D_{11}\cos^2\alpha+D_{22}\sin^2\alpha \quad (15)$$

$$D_y=D_{11}\cos^2\beta+D_{22}\sin^2\beta \quad (16)$$

$$D_x=D_{11}\cos^2(90-\beta)+D_{22}\sin^2(90-\beta) \quad (17)$$

β=orientation of fibers with respect to y axis

In the early stages of diffusion, i.e. when the ratio of the moisture absorbed to the maximum moisture content varies linearly with the square root of the time of exposure, there is no significant interaction between the diffusion of the different sides. Equation (8) can then be applied independently to each edge of the composite resulting in a diffusion coefficient corrected for edge effects [38].

$$D=D_z\left(1+\frac{h}{l}\sqrt{\frac{D_x}{D_z}}+\frac{h}{l}\sqrt{\frac{D_x}{D_z}}\right)^2 \quad (18)$$

For a laminated composite, Equations 15 to 17 become

$$D_z=D_{22}=D_r\left(1-2\sqrt{\frac{V_f}{\pi}}\right) \quad (19)$$

$$D_y=D_{11}\frac{\Sigma h_j\cos^2\beta_j}{\Sigma h_j}+D_{22}\frac{\Sigma h_j\sin^2\beta_j}{\Sigma h_j} \quad (20)$$

$$D_x=D_{11}\frac{\Sigma h_j\sin^2\beta_j}{\Sigma h_j}+D_{22}\frac{\Sigma h_j\cos^2\beta_j}{\Sigma h_j} \quad (21)$$

h_j=thickness of j^{th} ply

β_j=angle of j^{th} ply with respect to y axis

The preceding equations are based on Fickian diffusion. Non-Fickian moisture absorption behavior may be observed in several instances such as when moisture exposure occurs at elevated temperatures and microcracking develops [46,47] or when exposure occurs while the material is being mechanically stressed [40]. Some researchers have reported non-Fickian diffusion behavior for the 3501-6 resin following exposure above certain temperatures and humidities [46,47]. Collings and Copley found non-Fickian diffusion for conditioning temperatures above 60^{o} C (140^{o} F) or humidities above 96% RH [52]. However, Shirrell and Sandow observed non-Fickian diffusion in the 3501 resin only at combined conditions of elevated temperature (82^{o} C) and humidity. All the specimens that exhibited this anomaly had surface and edge microcracks [46]. In such cases, the water absorption may be higher than calculated by the Fickian model. An increase in the fraction of voids will also increase the moisture weight gain.

Matrix plasticization is only one effect of composite moisture absorption. Matrix swelling with moisture can also be significant. The swelling strains due to moisture are treated analogously to thermal strains.

$$\epsilon_m=\beta_m (C_f-C_i) \qquad (22)$$

ϵ_m=moisture swelling strain
β_m=moisture expansion coefficient
C_f=final moisture concentration
C_i=initial moisture concentration

Differential stresses can develop in a composite with a moisture gradient through the thickness as the outer layers expand and pull on the inside layers [48,49]. The effect of these swelling stresses may be positive or negative depending on whether they relieve or add to the residual stresses in the laminate.

CONDITIONED RESULTS

The available data on mechanical property changes in composite materials due to environmental conditioning has been generated primarily by the aircraft industry. Consequently, the environmental conditioning reflects aircraft operating conditions i.e. thin composite sections exposed to hot, humid environments.

Differences in exposure method, moisture content, materials, laminate orientations, temperature and loading condition make it difficult to draw general conclusions regarding the effects of environmental conditioning on composite mechanical properties. Decreases in compression strength ranging from 11% to 20% have been reported for thin graphite/epoxy laminates humidity conditioned at room temperature to 50% maximum saturation and higher [21,50,51 52]. The longitudinal elastic modulus of unidirectional laminates appears to remain unchanged with moisture at room temperature [38,50], but the transverse modulus drops by 12% [38].

Failure mode differences between dry and wet specimens are also of interest as they may provide insight into the differences in compression strengths between these specimens. Grimes and Adams [50] found a 20% drop in the static compression strength, and observed similar gross failure modes in the dry and wet (unidirectional

graphite/epoxy laminates with a 1% moisture content by weight). However, the wet specimens showed slightly more delamination than the dry specimens. Their specimens were tested with the IITRI compression fixture. Barker and Balasundaram [21] tested 2.00 mm (0.079 in.) thick laminates by end loading in compression, and found changes in failure mode in the 0° lamina of a $[(90/0)_4]_S$ laminate from shear in the dry material to fiber microbuckling in the wet material. These changes in failure mode were accompanied by a 12.5% drop in compression strength.

EXPERIMENTAL PROCEDURE

SPECIMEN FABRICATION AND PREPARATION

Four graphite/epoxy panels were fabricated from AS4/3501-6 prepreg (.005" nominal thickness). The fiber and epoxy properties are shown in Tables 1 and 2. Two panels were prepared with 48 plies to give a nominal 6.35 mm (0.25 in.) thickness when cured. The remaining two panels had 12 plies and a 1.6 mm (0.0625 in.) cured thickness. The time-temperature profile used in curing is shown in Figure 11. A symmetric $0_2/90$ layup was selected instead of a unidirectional layup to avoid difficulties due to transverse brooming expected with testing thick unidirectional coupons. The 90° reinforcement provides transverse constraint which aids development of the full material strength.

Each panel was inspected for delaminations and voids with an ultrasonic C-scan. Tag end samples were used for acid digestion to determine fiber volume fractions of 62% and 66% for the thick and thin panels, respectively [53]. Void contents using this technique were typically less than 1%. Specimens with the dimensions shown in Figure 12 were cut from each panel. The ends of each specimen were ground flat and parallel to a tolerance of $\pm$0.0254 mm ($\pm$0.001 in.) to minimize difficulties in loading due to uneven fiber ends. The gage length-to-thickness ratio (l:t

ratio) for the thick specimens was 3:1. This l/t provides a safety factor of 2.0 against Euler buckling assuming clamped ends and including transverse shear effects (see Appendix A). The same l/t ratio for the thin specimens means the gage length would be 4.7625 mm (0.1875 in.). This l/t ratio was used initially, but resulted in low strength failures at the specimen's exit from the grips. Consequently, the l/t ratio for the thin specimens was increased to 6.4:1 so that stress concentration effects from the grips would not extend throughout the entire gage length. The buckling safety factor for this l/t ratio was 1.1. Selected specimens of each group were strain gaged for modulus measurements with a single gage or back to back gages to monitor specimen alignment. CEA-06-125UW-350 gages were used on the 6.35 mm (0.25 in.) thick specimens with a gage length of 19.05 mm (0.75 in.). The strain gages were applied immediately prior to testing with a cyanoacrolate adhesive. The same procedure was followed for the thin specimens using CEA-06-062UT-350 gages to accomodate the shorter gage length.

One objective of this investigation was to compare dry and wet specimen behavior. This required moisture conditioning of half the specimens. The specimens to be moisture conditioned were first dried repeatedly in a 50° C (122° F) oven until there was less than a 0.5% change in specimen weight before and after drying. After

conditioning, the specimens were stored in room temperature water until testing. This was done to prevent surface drying which could result in detrimental differential stresses between a swollen wet core and the dry outside surface [46]. The room temperature diffusion coefficient for AS4/3501-6 is fairly small, so any additional water absorption due to this storage method should be minimal. All specimens were usually tested within a week of conditioning. Strain gages were applied after surface drying and immediately prior to testing.

100 grit sandpaper tabs were bonded onto the gripped portions of the specimens with a cyanoacrolate adhesive. A 6.35 mm thick specimen with sandpaper tabs is shown mounted in the compression fixture in Figure 6. Initial specimen testing without the sandpaper resulted in a disproportionate number of end failures at low strengths. The sandpaper was added to obtain a partial shear transfer of the load by increasing the frictional force between the specimen and the fixture. Similar difficulties with end failures were also encountered by Reference 19 who concluded that 20% of the axial load had to be transferred by shear to avoid end failures.

An estimate of the frictional effects due to the sandpaper was obtained in the following manner. The force required to push the specimen through the fixture with and without sandpaper was recorded (see Figure 13). The

coefficient of friction without sandpaper was .15 and the coefficient of friction with sandpaper was .08. This means that the per cent load transferred by shear was 48% without sandpaper and 25% with sandpaper. It is apparent from these measurements that the sandpaper did not increase the frictional force between the fixture and the specimen. However, the use of sandpaper eliminated the low strength failures possibly by reducing the stress concentration where the specimen exited the steel clamping blocks.

ENVIRONMENTAL CONDITIONING

The thick specimens for moisture conditioning were exposed to distilled water at 100° C (212° F) for 29 days using the experimental arrangement illustrated in Figure 14. The temperature of 100° C (212° F) was chosen so that significant water absorption could be induced for the thicker specimens in a reasonable amount of time.

Each specimen was surface dried and weighed after conditioning. SEM examination of a few thick specimens following conditioning showed no evidence of microcracking. The average per cent weight gain (M) due to moisture absorption for the thick specimens was 1.86%. The per cent weight gain following one month's exposure to 100° C distilled water was predicted using Equations (12) and (13). Solving for M in these equations required the diffusion coefficient (D), the initial moisture content (M_i) and the maximum composite moisture content (M_m).

The diffusion coefficient (D) in Equation (13) was determined as shown in Appendix B. The magnitude of this coefficient changes with the inclusion of edge effects which occur when the thickness of the specimen becomes a significant fraction of its in-plane dimensions. The diffusion of moisture through all six sides of a rectangular coupon must then be considered [38]. Since the cut edges of the specimens in this study were not sealed against moisture absorption, edge effects had to be

included in this analysis.

The specimens were oven dried prior to conditioning to eliminate the initial moisture content. The maximum possible moisture content in a composite laminate is the product of its resin weight fraction and the saturation moisture content of the neat resin [41]. Since the thick specimens had a resin weight fraction of 30%, and the reported values of the saturation moisture content of the Hercules 3501-6 neat resin range from 5.5% to 6.9% [41,54], it is evident that the maximum moisture content of the thick laminate ranges between 1.65% and 2.09%. The measured moisture content of 1.86% fell within this range indicating that the thick laminates were probably saturated.

Ideally, comparison of the wet thick and thin laminate compression behavior should be based on both laminates having the same moisture content. However, the resin weight in the thin laminates was 27% compared to the 30% resin weight in the thick laminates. Following the process previously described, the saturation moisture content of the thin laminates would be less than that of the thick laminates, and range from 1.5% to 1.9%. Actually, the thin specimens exhibited weight gains of 1.3% after five days of exposure to 100^{o} C distilled water. These weight gains did not change significantly even with continued exposure for a total of seventeen

days.

The measured saturation moisture content in the thin laminates was slightly below that predicted using Equation (11). Several factors must be considered when comparing predicted and measured moisture absorption values. First, the predicted values require accurate knowledge of the material diffusion coefficient. It is not uncommon for composite diffusion coefficients reported in the literature to be based on data with 20% or more scatter [38,55]. Secondly, the resin weight fraction and composite void content must be accurately determined. Both of these values are typically determined by acid digestion techniques, which was the method used in this study.

The first step in acid digestion is to measure the volume of water displaced by the material sample. The resin is then separated from the fiber by soaking the composite in nitric acid. This step allows the resin and fiber weight fractions to be measured. If the fiber and resin densities are known, their respective volume fractions can be calculated. The difference between the sum of the resin and fiber volume fractions and the total volume of water displaced by the sample is the volume void content in the composite sample. The composite void content obtained with this method depends on the accuracy of the fiber and resin densities, and on the precision of the measurement of the volume of water displaced by the

composite laminate. Comparison of void contents measured by acid digestion with those from image processing techniques showed that acid digestion methods consistently underestimated the volume of voids [8]. If there is a large percentage of trapped voids in the resin in the composite, more moisture could be absorbed than would be expected based on neat resin data where the resin was presumably void free.

All the specimens will be considered saturated in this study. This assumes that the differences in moisture absorption between the thick and thin specimens are due to their different resin contents. In addition, the thin specimens absorbed less moisture than predicted, but since they showed no appreciable change in moisture content between five and seventeen days of moisture exposure, it is not unreasonable to assume these specimens were saturated.

COMPRESSION TEST FIXTURE

An end loading compression fixture developed at the David Taylor Research Center by Camponeschi [9] was selected for compression loading based on its capacity for testing 6.35 mm (0.25 in.) thick laminates, and for the simple specimen geometry required. The fixture, shown in Figure 6, and illustrated schematically in Figure 15, consists of two hardened steel clamping blocks each held together by four M6.35 x 1.27 screws. The blocks are 76.2 mm x 63.5 mm x 44.5 mm (3.0 in. x 2.5 in. x 1.75 in.). Guidepost slots with linear bearings are employed to maintain the fixture alignment. Preliminary trials with the fixture showed that the guideposts were needed only for the thin specimens. The thick specimens were easily assembled in the fixture with no guideposts, and back-to-back strain gages on these specimens during testing showed no evidence of bending. Guideposts were required for assembly of the fixture with the thin specimens. Without guideposts, failures occurred during assembly as the second clamping block was mounted and tightened on the specimen. This caused bending and failure of the specimen.

TEST PROCEDURE

Each specimen was mounted in the fixture with the M6.35 x 1.27 bolts tightened to a 20.25 J torque. If the bolts were only hand tightened, transverse brooming at the specimen ends almost always occurred at relatively low loads. The load was applied at a rate of 1.27 mm/mm/min (0.05 in./in./min.) using a 60 kip Satec universal machine, with a spherically seated compression platen for alignment purposes. At least ten specimens in each of the four series were tested to failure.

RESULTS

The mean dry thick compression strength was 1055 MPa ± 19 MPa (151 ksi ± 3 ksi) compared to 1090 MPa ± 70 MPa (156 ksi ± 10 ksi) mean strength of the dry thin specimens. The reported ranges for these mean strengths were calculated using a Student t distribution to compensate for the small sample size. They indicate that the probability that the population mean will be located within this range is 95% [56]. Statistically, there was no significant difference between the mean strengths of the dry thick and thin specimens. The wet strengths of each set of specimens were significantly lower than their dry strengths. The mean thick wet strength was 740 MPa ± 52 MPa (106 ksi ± 7 ksi). The mean thin wet strength was 957 MPa ± 75 MPa (137 ksi ± 11 ksi). The compression strength data for the thick and thin specimens is shown in Tables 3 and 4.

Stress-strain curves for the dry and wet specimens are shown in Figures 16 through 19. Due to the small sample size, no statistical analyses were performed on these populations. The dry specimens (both thick and thin) had initial modulus values of 80 GPa (11.5 Msi), as did the thick wet specimens. The stress-strain data for the thin wet specimens, presented in Figure 19, has significant scatter with most of the initial modulus values at 98 GPa (14 Msi). All the observed stress-strain curves showed

slight nonlinearities typically beginning at 40-50% of the ultimate compressive load.

Typical thick and thin failure modes for both the dry and wet specimens are shown in Figures 20 through 23. Figures 20 and 21 show little difference in the gross failure mode between the thick dry and wet specimens. Each was characterized by delamination and angular cracking across the specimen thickness to the midplane. Overall, delaminations were greater in the wet specimens. They occurred on the outside surfaces and throughout the thickness of the specimen, often extending from the gage section to the gripped area of the specimen. The crack angles across the thickness ranged from 27^{o} to 30^{o} for both dry and wet specimens, as measured from an axis perpendicular to the longitudinal axis of the specimen. Occasionally, biangular cracking across the specimen thickness was observed with the mirror image cracks meeting in a peak at the specimen midplane. Failures also occurred on some specimens at the ends at strengths equivalent to those specimens that failed in the gage section. The failures at the ends usually exhibited multiple cracks through the thickness, again at angles of 27^{o} to 30^{o} for both the wet and dry thick laminates.

The failed thin wet and dry specimens, pictured in Figures 22 and 23, also appeared very similar with

slightly more delamination seen in the wet specimens. Direct comparison to their thick counterparts is difficult due to the greater amount of damage at failure in the thin specimens. The thin specimens never exhibited clean angular cracks through the thickness as observed in the thick specimens. Scattered cracks across the 90° midplane plies were observed in some of the thin wet specimens as illustrated in Figure 23. Occasionally, these cracks were connected to a delamination between the 90° and 0° plies. Such cracking was not observed in the thin dry specimens.

ANALYSIS

GLOBAL FINITE ELEMENT ANALYSIS

MESH AND BOUNDARY/LOAD CONDITIONS

Three dimensional linear finite element analyses of the dry and wet specimens were performed to evaluate changes in the stress state from swelling strains and matrix softening due to moisture absorption. The finite element code chosen for the analysis was ABAQUS written by Hibbitt, Karlsson, and Sorensen. It is a general purpose program featuring a number of capabilities that include static stress, dynamic stress, heat transfer and buckling analysis options. Non-linearities may be introduced in the stress analysis with non-linear constitutive relations that describe the material (isotropic materials), or by geometric or boundary (contact) non-linearities [57].

The finite element model of the compression specimen and test fixture was simplified to minimize computational costs. Symmetry about the x-y, the y-z and the x-z planes reduced the model to one-eighth of the actual specimen size as shown in Figure 24. The finite element mesh for this model, shown in Figure 25, consisted of 368 20-node isoparametric brick elements. As a first approximation, clamping of the specimen by the fixture was modeled by setting the nodal displacements in the y direction equal to zero in the shaded region of Figure 26. The

compression load on the specimen was applied as concentrated nodal forces to the nodes of surface A.

COMPOSITE MATERIAL REPRESENTATION

Ideally, a finite element model of a composite laminate would be constructed on a ply by ply basis. The elements of each ply could then be represented as separate orthotropic materials with their material properties depending on the orientation of the ply within the laminate. This approach requires that each ply have at least one element through its thickness which forces a large number of elements to be used in the other directions to keep element aspect ratios reasonable. For example, a graphite/epoxy ply is typically 0.127 mm (0.005 in.) thick, so that a 73.00 mm x 6.35 mm x 3.18 mm (2.875 in. x .25 in. x .125 in.) model would require over 700,000 3-D elements if the aspect ratio of the elements is 1:1. Such an approach is currently unrealistic for thick laminates as the large number of plies would make the number of elements too large for a 3-D analysis to be conducted at a reasonable cost. Consequently, in this analysis, "smeared" orthotropic properties were used. It was assumed that the "smeared" material would have the same global response as the material modeled on a ply by ply basis [58].

MOISTURE EFFECTS

Two changes were made in the model to accommodate the moisture conditioned specimens. First, the smeared material properties were adjusted to account for the loss of stiffness in the unidirectional transverse modulus due to moisture. This adjustment involved a reduction in the transverse Young's modulus (E_2 and E_3) of dry AS4/3501-6 [59] by 12% to get the unidirectional wet lamina properties. The reduction of 12% was selected based on experimental data reported by Chi-Hung and Springer [60] for AS4/3501. The $(0_2/90)_s$ cross ply laminate smeared material properties were then obtained using STIF3D which is PC-based program developed at the University of Delaware [61]. The effective homogeneous constitutive equations used in STIF3D were originally reported by Pagano [62], and include the effects of bending-extensional coupling. The resultant 3-D unidirectional and cross ply material properties for the dry and wet material are shown in Table 5. Since the cross ply laminate is dominated by the 0^o plies, stiffness reductions in the unidirectional transverse modulus did not significantly affect the smeared material properties.

The second change made in the model to represent the effects of moisture was the incorporation of swelling strains. For a unidirectional AS4/3501 lamina, the coefficient of moisture expansion, β, (analagous to the

coefficient of thermal expansion) as reported by Tsai [63] is negligible in the fiber direction. In the transverse and through thickness directions β is 0.44 $\%M^{-1}$. The moisture expansion coefficients for a $(0_2/90)_s$ laminate, based on classical laminated plate theory are then 0.147 $\%M^{-1}$ in the 0^o direction, 0.293 $\%M^{-1}$ in the 90^o direction and 0.44 $\%M^{-1}$ through the thickness.

Multiplication of the coefficient of moisture expansion by the moisture concentration yields the swelling strain which can then be superimposed on the mechanical strains due to the compressive load. Generation of the moisture concentration profile through the specimen thickness was based on Fickian diffusion and corrected for edge effects using the methodology presented by Springer [38]. All calculations are shown in Appendix B. The moisture concentrations as a function of position through the thickness of both the thick and thin specimens are shown in Figures 27 and 28 for two exposure time periods. These results show that the distribution of the moisture concentration was nearly constant for the thick and thin specimens.

Thermal strains associated with a temperature differential are easily calculated in ABAQUS. Since swelling strains are analogous to thermal strains, the moisture concentration data from Figures 27 and 28 was simulated in ABAQUS as a temperature distribution, and the

moisture expansion coefficients were simulated as thermal expansion coefficients. Since the moisture gradients were very small, and the changes in the elastic constants were moderate, large differences between the wet and dry analyses were not expected.

RESULTS

The distribution of the stresses (three normal and three shear) showed only minor differences between the stress state existing in the wet and dry specimens. The longitudinal stress (σ_z) was typically two to three orders of magnitude greater than the remaining stresses ($\sigma_y, \sigma_x, \tau_{xy}, \tau_{xz}, \tau_{yz}$) in both the wet and dry specimens. Slight increases in σ_x and σ_y occurred due to the addition of moisture, but the overall magnitude of the stresses, σ_x and σ_y, remained small (less than 7 MPa).

MICROMECHANICAL ANALYSIS

BACKGROUND

In addition to the global stress analysis conducted using ABAQUS, a micromechanic analysis was conducted to compare the compression strength of wet and dry specimens. As discussed in the literature review, the compression failure theory of Reference [6] was chosen for this comparison. Use of this failure theory requires the shear stresses in the matrix as a function of the compressive load on the composite laminate. The approach presented in Reference [6] to determine the matrix shear stresses served as a guideline for the analysis in this study, and will therefore, be briefly discussed.

In [6], a composite laminate was modeled as a multilayered Timoshenko beam that permitted transverse deflections of each layer and allowed the cross sections to rotate with respect to the neutral axis. Using this model, two cases were considered. The first case represented the entire laminate as alternating fiber and matrix layers. Since this was not practical for thicker laminates, a second case was evaluated which consisted of a fiber layer surrounded by two matrix half layers, representing a repeating structure within the laminate. Expressions for the displacement of each layer were obtained using multilayered Timoshenko beam theory. These diplacements represented those due to bending and shearing

of the cross-section. The axial displacements due to the axial compressive load on the beam were ignored. Displacements were converted to strains using the strain-displacement equations, and Hooke's law was used to convert the strains to stresses. A set of linear second order partial differential equations for this problem were then developed using the equilibrium relations. These equations were expressed in finite difference form and solved numerically. The nonlinearity of the matrix material was incorporated in the analysis by dividing the matrix shear stress-strain curve into a number of linear segments. Loads were then applied incrementally with variations in the matrix shear modulus occuring within the load increments. An initial imperfection in the beam was allowed and mathematically described by

$$w_o = a_o\{1+\sin[(\frac{2\pi}{L})(x-\frac{L}{4})]\} \qquad (23)$$

w_o= amplitude of imperfection as a function of length along the beam

a_o= half the maximum amplitude of the imperfection

L= length of the beam equivalent to half the wavelength of the imperfection

The solution of the governing set of differential equations yielded displacements which could be used to calculate the shear stresses in each layer.

The shear stresses obtained with the preceding

solution depended on which case (entire laminate or repeating element) was modeled. The repeating element model typically predicted shear stresses that were 15-20% lower than those predicted with a model of the entire laminate [33]. The difference in the predicted shear stresses between the two models increased with a decrease in the fiber to matrix longitudinal modulus ratio.

Two failure theories were developed based on these calculated shear stresses. If the shear stress in the matrix layer exceeded the interlaminar shear strength of the material, failure would occur by delamination. The second mode of failure was shear buckling. Assuming that the lamina length-to-width ratio was small enough to preclude Euler buckling, Davis postulated that the change in strain energy from the initial to the final position was due solely to shearing strains. Equation (5) is the resultant expression for the critical axial compressive load leading to shear instability.

The compression strength of the composite is based on the shear moduli of the fiber and matrix and their respective volume fractions. Since the fiber shear modulus and volume fraction do not change with moisture absorption, the matrix shear modulus will be the critical parameter. Accurate use of this failure theory is then dependent on two factors. First, the matrix shear stress-strain curve must be known as a function of moisture. And

secondly, the correct matrix shear modulus corresponding to the shear stress-strain state of the matrix must be chosen.

MESH AND BOUNDARY CONDITIONS

In this analysis, the shear stresses in the matrix of a composite loaded in compression were determined with finite element techniques (ABAQUS program) versus finite difference methods. Axial displacements due to axial compression were included in the analysis. Two models of the composite laminate were considered. In the first case, a repeating element within the laminate was modeled as a fiber plate surrounded by two half layers of matrix. The fiber and matrix layer thicknesses were proportional to their respective volume fractions within the ply. The total thickness of the beam was equal to one ply thickness 0.127 mm (0.0055 in.). This model was very similar to Davis' repeating element case for modeling boron/epoxy composites. However, the diameter of a boron fiber is approximately fourteen times that of a graphite fiber, so modeling the fibers in a boron/epoxy ply as a single fiber plate is reasonable. Since the graphite fibers are so small in diameter, many fibers will be stacked through the ply thickness, so the single fiber plate model might not reflect interactive effects between fibers. Therefore, a second model was also included in this analysis which

consisted of two fiber plates separated by a matrix layer and surrounded by matrix half layers. The total fiber and matrix layer thicknesses were again proportional to their respective volume fractions within the ply. A 4400 element mesh was used for each of these models and is shown in Figure 29. The elements were second order (8 node) plane strain, isoparametric quadrilaterals.

The initial imperfection in the fiber-matrix beam was generated using Equation (21) with two amplitude-to-length ratios, 0.00375 and 0.009. These ratios were chosen somewhat arbitrarily as data on initial imperfections in flat graphite/epoxy laminates is not extensively available. The lower ratio represents amplitudes measured by Davis for boron/epoxy laminates, and Camponeschi for graphite/epoxy laminates [33,64]. Significantly higher ratios (0.025) were used by Hyer and Telegadas to represent waves in graphite/epoxy filament wound cylinders [7,65]. Imperfections this large would be unlikely in a flat laminate. The ratio of 0.009 was chosen as a midway point between wave amplitudes seen in flat plates and filament wound cylinders, and to illustrate the effects of an increasing wave amplitude on the predicted shear stresses in the matrix.

The beam length (or half wavelength) was 0.76 mm (0.03 in.), which is equivalent to half the critical length for Euler buckling. This resulted in a beam

length-to-thickness ratio of 5.5:1. No attempt was made to evaluate the effects of variations in wavelength on the magnitude of the shear stresses at the fiber-matrix interface.

Uniform axial displacements corresponding to 1.5% strain for the dry specimens and 1.2% strain for the wet specimens were imposed on one end of the beam while the other end was held fixed. The model had been sized to avoid Euler buckling, but the analysis was geometrically non-linear allowing for large displacements and rotations should they occur due to material property changes. Therefore, no symmetry boundary conditions were used.

The top and bottom surfaces of the model were free to move in the x and y directions. In actuality, some type of normal and shear forces are exerted on these surfaces by the plies above and below the repeating element. The boundary conditions on these surfaces are difficult to describe, particularly in the presence of a wavy ply. Davis [33] fixed the axial displacement of the nodes on these surfaces. Hyer and Telegadas [65] modeled several layers above and below a wavy ply, and then used an elasticity solution for boundary conditions away from the wave.

Neither of these conditions were appropriate for the model in the current analysis which differed slightly from the preceding models. Preliminary trials with the current

model showed a reduction in shear stress with the addition of any normal forces on the top and bottom surfaces of the model. Therefore, no constraints were placed on the nodes on these surfaces in an attempt to simulate a worst case scenario.

MATERIAL MODEL

The fiber was modeled as a transversely isotropic material with the properties shown in Table 1. A three parameter Richard-Blacklock equation was used to describe the nonlinear shear behavior of the matrix [48]. The relationship established between shear stress and shear strain is shown in Equation (22).

$$\tau = \frac{G\gamma}{[1+(\frac{G\gamma}{\tau_0})^n]^{\frac{1}{n}}} \qquad (24)$$

G= initial shear modulus
n= curvature parameter
τ_0= asymptotic shear stress value

Adams developed expressions for the parameters in Equation (24) as functions of temperature and moisture [49]. The matrix shear stress-strain curves generated using this model are shown in Figure 30 for the dry and wet (matrix moisture contents corresponding to 1.3% and 1.9% moisture contents by weight in the composite laminate) material. If the shear stress in the matrix is known as a function of axial compressive load, the proper modulus can be

chosen from these curves for use in Equation (5). The finite element analyses were performed with the matrix material behaving linear in shear. An attempt was made to bound the solution by using three values for the matrix shear modulus (initial dry, intermediate, and final wet) for each amplitude to wavelength ratio. These modulus values were 1.6 GPa (.23E6 psi), 0.99 GPa (.1415E6 psi) , and 0.37 GPa (0.53E5 psi), respectively. This covered the range of matrix shear modulus values from its stiffest value (initial dry modulus) to its softest value (final wet modulus). The analysis with a uniform axial displacement corresponding to a strain of 1.2% (wet specimens) was performed using only the intermediate matrix modulus value for both amplitude to length ratios.

RESULTS

Stresses in the global coordinate system were obtained at the integration points from the finite element analysis. The through thickness shear stresses were expected to be continuous based on classical laminated plate theory which assumes equal and opposite traction boundary conditions between plies for the out-of-plane stresses [66]. However, this required a rotation of the stresses from the global coordinate system to a local coordinate system normal and tangential to the element edges [7,65]. The highest matrix shear stresses were

expected to occur at the fiber-matrix interface.

The maximum interfacial shear stresses occurred at points one-fourth and three-fourths the length of the beam for both the single fiber and double fiber plate models. The matrix and fiber shear stresses at these quarter points A (Figure 29 a) and b)) in the single and double fiber plate models were very similar. However, in the double fiber plate model, the matrix shear stresses at point B in Figure 29 b) were typically 8 to 22 times greater than the matrix shear stresses at point A. These results indicated that interactive effects resulting from many fibers stacked through the ply thickness could have a significant effect on the predicted matrix shear stresses. Therefore, the double fiber plate model was chosen as the prototype for this study. The maximum matrix shear stresses in this model occurred along the C-D interface shown in Figure 29.

The maximum shear stresses (at the integration points) in the fiber and matrix elements on either side of the C-D interface are shown in Figures 31 and 32 for both amplitude-to-wavelength ratios. To be conservative, an average of the shear stresses from the fiber and matrix integration points on either side of the interface was chosen to represent the maximum shear stresses in the matrix at the interface. Additional mesh refinement at the interface would be required to predict the interfacial

shear stresses more exactly. Table 6 lists the maximum shear stresses from each of the analyses which will be used to select tangent shear moduli from the matrix shear stress-strain curves in Figure 30. These tangent shear moduli will then be used in Equation (5) to predict the compression strength of the graphite/epoxy laminates.

DISCUSSION AND CONCLUSIONS

Experiment

End loading compression techniques have given lower compression strengths for composites as compared to shear loading methods (IITRI and Celanese compression tests, for example). Since the laminate strengths in this study were generated using end loading techniques, it was important to establish some confidence in the test method by comparing these results with the strength determined by other methods.

The mean laminate compressive strengths were 1055 MPa (151 ksi) and 1090 MPa (156 ksi) for the dry thick and thin laminates, respectively. Using classical laminated plate theory [62], a unidirectional longitudinal compressive modulus of 119 GPa (17E6 psi) [9], and a unidirectional transverse compressive modulus of 10 GPa (1.5E6 psi) [66], the critical stress was 1484 MPa (212.5 ksi) and occurred in the 0^{o} plies of the $(0_2/90)_s$ laminate. Compressive unidirectional lamina strengths for AS4/3501-6 generated using the IITRI compression fixture range from 1397 to 1537 MPa (200 to 220 ksi) [21,23,28,50]. Since the stresses developed in the 0^{o} plies in this study were within this range, it was concluded that the test method developed was satisfactory.

The literature review indicated that a drop (20% or less) in compression strength was expected after moisture

conditioning to saturation. We found that the wet laminate strengths were 11% and 30% lower than the dry laminate strengths for the thin and thick specimens, respectively. The larger loss of strength in the thick laminates may be due to the greater amount of moisture absorbed by these specimens. Linear extrapolation of the strength of a specimen with 1.3% moisture to one with 1.86% moisture (observed in the thick laminates) results in a drop in the compresssion strength to 678 MPa (97 ksi). This prediction is consistent with the actual strengths observed in the wet thick laminates.

Moisture had little effect on the fiber dominated longitudinal modulus between 0% and 0.2% strain in the thick laminates. The thin laminates showed an increase in longitudinal modulus after moisture conditioning which is not consistent with any cases reported in the literature. It appears that the outer plies of the thin wet laminate buckled, and the strain gage sensed tensile strains due to bending. These tensile strains, in the presence of the compressive strain due to the longitudinal load, lead to a smaller combined strain measurement (and higher modulus) as compared to the case with no outer ply buckling.

A comparison in the gross failure mode of the wet and dry specimens in Figures 20 through 23 for the thick and thin laminates showed little difference except for slightly greater delaminations in the wet specimens. These results

are similar to those reported by Grimes and Adams [50]. The catastrophic nature of the final failure destroyed any clues as to the failure mechanisms immediately preceding final failure that might be determined by microscopic examination. It is possible that different mechanisms initiated failure in the wet and dry laminates, but that the gross features of the failure appeared the same.

The thick specimens typically exhibited a combination of delamination and angular cracking through the laminate thickness. Similar failure modes under compressive loading have been observed in dry graphite/epoxy by Smoot [23], Garala [25] and Camponeschi [64]. The crack angles through the thickness ranged from 27^{o} to 30^{o} for both the wet and dry thick laminates. These angles are consistent with the 26^{o} kink band angles reported by Hahn [1] for graphite/epoxy composites.

The angularly cracked surfaces were not observed following failure in the thin specimens. The majority of these specimens had significant damage in the failure zone making identification of the failure mode difficult. The wet specimens exhibited more delamination, and a few showed significant cracking across the 90^{o} midplane plies. This may be a result of reduced matrix properties due to moisture absorption.

Theory

The differences in stress states predicted by the 3-D finite element analysis for the wet and dry laminates did not explain the large differences in strength measured in the laboratory. This result was expected because the moisture gradients modeled in the analysis were small, and large differences in the stresses between the swollen wet layers and the dry layers did not develop.

Since moisture absorption in a composite material occurs in the matrix, it is not unreasonable to assume that changes in matrix behavior with moisture are linked to the compression strength differences of the dry and wet laminates. A finite element analysis on the constituent level was performed to determine the shear stresses at the fiber-matrix interface in a composite ply loaded in compression. Initial waviness of the ply was incorporated in the model. The maximum interfacial shear stress from the analysis was used to select a tangent modulus from the wet and dry matrix shear stress-strain curves. The appropriate tangent shear modulus was then used in Davis' [6] compression failure theory (Equation (5)) based on shear instability.

The micromechanical analysis showed maximum matrix shear stresses ranging from 34 MPa (4.8 ksi) to 65 MPa (9.3 ksi) for an initial imperfection amplitude to wavelength ratio of 0.00375, and from 70 MPa (10.0

ksi) to 140 MPa (20.0 ksi) for a ratio of 0.009 (See Table 6). The upper bound of each range occurred when the initial dry matrix shear modulus was used in the analysis, and the lower bound occurred with the use of the final wet modulus. Since the matrix shear stress-strain behavior is highly nonlinear, use of these moduli might overestimate or underestimate the actual matrix shear stresses. Therefore, analyses were also run with an intermediate matrix shear modulus. Predicted matrix shear stresses then ranged from 54 MPa (7.8 ksi) to 112 MPa (16.0 ksi) for the 1.5% strain case and from 44 MPa (6.2 ksi) to 91 MPa (13.0 ksi) for the 1.2% case.

The upper bound stress from each of these ranges exceeds the reported maximum interlaminar shear strength of 91 MPa (13.0 ksi) for the dry material and 70 MPa (10.0 ksi) [67] for the wet material. A wave amplitude to length ratio of 0.009 was used to predict the upper bound stresses. This ratio may be too large for autoclave cured laminates. The upper bound stress of each range was reduced to the appropriate (dry or wet) interlaminar shear strength. However, predicted matrix shear stresses were of sufficient magnitude to indicate that delamination was also a possible failure mode for these laminates. Experimental observations of combined failure modes (delamination and shear cracking through

the specimen thickness) support this conclusion.

The failure stresses determined experimentally are compared with the stresses predicted from Equation (5) in Table 7. Two predicted stresses are shown. The first uses a matrix tangent shear modulus corresponding to the lower bound matrix shear stresses, and the second uses a matrix shear modulus at the interlaminar shear strength of the material. The second prediction correlates best with the experimental results.

CONCLUSIONS

The compression behavior of thick (6.35 mm) $(0_2/90)_s$ AS4/3501-6 laminates was compared to that of thin (1.6 mm) section laminates in both dry and moisture saturated states. Experimental results showed no statistical difference in strength of the dry material of either thickness. However, there was a statistically significant difference in the strengths of moisture conditioned specimens of different thicknesses. The thick specimens absorbed significantly more water than the thin specimens, and consequently, showed a greater loss in compression strength. This experimental observation was substantiated with a stress analysis that accounted for the reduced matrix properties of the thicker specimens associated with the higher moisture content.

Slightly more delamination was observed in the wet

specimens of both thicknesses. The thick laminates exhibited a combination of delamination and angled cracks of 27^{o} to 30^{o} partially across the thickness of the specimen. Comparison of the failure modes of the thick and thin laminates was difficult due to the extensive delamination and damage that occurred in the thin laminates. Well defined angular cracks, as seen in the thick specimens, were not observed.

No change in longitudinal modulus was observed with moisture concentration or with thickness.

Strength differences between the dry and wet laminates are not due to moisture induced stresses. It appears that the detrimental influence of the moisture is the degradation of the matrix shear modulus at high compressive stresses with high moisture concentrations.

APPENDIX A BUCKLING LOAD

The equation used to calculate the global buckling stresses for the compression specimens was derived by Timoshenko and included transverse shear effects [68]. Clamped-clamped end conditions were assumed.

$$\sigma_{cr} = \frac{E_x \pi^2}{12\left(\frac{l}{t}\right)^2 + \pi^2 1.2 \frac{E_x}{G_{xz}}} \qquad \text{(A-1)}$$

σ_{cr}= critical buckling stress
E_x= longitudinal modulus
l= unsupported length
t= specimen thickness
G_{xz}= transverse shear modulus

For AS4/3501-6 in a $(0_2/90)_s$ layup, the longitudinal modulus is 84 GPa (12E6 psi), and the transverse shear modulus is estimated at 3.5E6 GPa (.5E6 psi). These modulus values were not changed for the conditioned specimens as a large effect on the longitudinal modulus was not expected for this particular layup. Safety factors were based on an estimated failure strength of 1048 MPa (150 ksi).

Thick Specimens $\frac{l}{t}$= 3 σ_{cr}= 2109 MPa (302 ksi) S.F.=2.0

Thin Specimens $\frac{l}{t}$= 6 σ_{cr}= 1152 MPa (165 ksi) S.F.=1.1

APPENDIX B MOISTURE CONCENTRATION

Prediction of the distribution of the moisture concentration through the thickness of the specimen requires a diffusion coefficient which takes into account edge effects and laminate orientation. Accounting for edge effects was necessary in this program because the specimen edges were not coated during immersion in 100° C (212° F) distilled water.

Calculation of the resin diffusion coefficient is the first step in estimating the diffusion coefficient for the composite laminate. An empirical expression for the diffusion coefficient of a unidirectional AS4/3501 composite with a fiber volume fraction of 65% immersed in distilled water is given in Equation B-1 [38].

$$D_c = 768 e^{\frac{-7218}{T}} \qquad \text{(B-1)}$$

D_c= composite diffusivity in $\frac{mm^2}{s}$
T= temperature in Kelvin

The resin diffusivity is given by

$$D_R = \frac{D_c}{1-2\sqrt{\frac{V_f}{\pi}}} \qquad \text{(B-2)}$$

D_R= resin diffusivity in $\frac{mm^2}{s}$
V_f= fiber volume fraction

For 100° C exposure,

D_c= 3.0286E-6 $\frac{mm^2}{s}$ (1.6900E-5 $\frac{in^2}{hr}$)

D_R= 3.3550E-5 $\frac{mm^2}{s}$ (1.8721E-4 $\frac{in^2}{hr}$)

Springer derived the following expression for the diffusion coefficient of a laminated coupon including edge effects [38].

$$D= D_R(1-2\sqrt{\frac{V_f}{\pi}})\left[1+\frac{h}{l}\sqrt{\frac{(1-V_f)\Sigma h_j\cos^2\beta_j}{(1-2\sqrt{\frac{V_f}{\pi}})\Sigma h_j}+\frac{\Sigma h_j\sin^2\beta_j}{\Sigma h_j}}\right.$$

$$\left.+\frac{h}{n}\sqrt{\frac{(1-V_f)\Sigma h_j\sin^2\beta_j}{(1-2\sqrt{\frac{V_f}{\pi}})\Sigma h_j}+\frac{\Sigma h_j\cos^2\beta_j}{\Sigma h_j}}\right]^2 \qquad \text{(B-3)}$$

β_j= $90^0-\gamma_j$ (See Figure 10)

j= 1 to N, N= number of plies in laminate

For a $(0_2/90)_s$ layup, Equation B-3 reduces to:

Thick Specimens

Σh_j= 6.35 mm (0.25 in.)

$\Sigma h_j\cos^2\beta_j= \frac{2}{3}(6.35)$

$\Sigma h_j\sin^2\beta_j= \frac{1}{3}(6.35)$

$$D=.11D_R(1+1.624\frac{h}{l}+ 1.348\frac{h}{n})^2 \quad V_f=.62 \qquad \text{(B-4)}$$

Thin Specimens

Σh_j= 1.6 mm (0.0625 in.)

$\Sigma h_j\cos^2\beta_j= \frac{2}{3}(1.6)$

$\Sigma h_j\sin^2\beta_j= \frac{1}{3}(1.6)$

$$D=.07D_R(1+1.839\frac{h}{l}+ 1.480\frac{h}{n})^2 \quad V_f=.68 \qquad \text{(B-5)}$$

For the thick specimens, $\frac{h}{l}=\frac{6.35}{146}$ $\frac{h}{n}=\frac{6.35}{12.7}$

$$D_{thick}= 1.123E\text{-}5 \frac{mm^2}{s}(6.265E\text{-}5\frac{in^2}{hr})$$

For the thin specimens, $\frac{h}{l}=\frac{1.6}{136.5}$ $\frac{h}{n}=\frac{1.6}{12.7}$

$$D_{thin}= 3.418E\text{-}6 \frac{mm^2}{s}(1.907E\text{-}5 \frac{in^2}{hr})$$

A computer program was written to calculate C(z,t) from Equation (9) in the main text using these diffusion coefficients.

REFERENCES

1. Hahn, H.T. and Williams, J.G., "Compression Failure Mechanisms in Unidirectional Composites," Composite Materials: Testing and Design (Seventh Conference), ASTM STP 893, J.M. Whitney, Ed., American Society for Testing and Materials, Philadelphia, 1986, pp.115-139.

2. Kumar, S., "Compressive Strength of High Performance Fibers," The Materials Science and Engineering of Rigid-Rod Polymers, W.W. Adams, R.K. Eby, D.E. McLemore, eds., Materials Research Society Symposium Proceedings, Vol. 134, Pittsburgh, Pa., 1989, pp. 1-12.

3. Elkin, Robert A., "Compression Testing of NOL Rings," Symposium on Standards for Filament Wound Reinforced Plastics, ASTM Special Technical Publication No. 327, June 1962.

4. Fried, N., "The Compressive Strength of Parallel Filament Reinforced Plastics--The Role of the Resin," Proceedings 18th Annual Technical and Management Conference, Reinforced Plastics Division, Society of Plastics Ind., Inc., February 1963.

5. Fried, N. and Kaminetsky, J., "The Influence of Material Variables on the Compressive Properties of Parallel Filament Reinforced Plastics," Proceedings 19th Annual Technical and Management Conference, Reinforced Plastics Division, Society of Plastics Ind., Inc., February 1964.

6. Davis, J.G., Jr., "Compressive Strength of Fiber-Reinforced Composite Materials," Composite Reliability, ASTM STP 580, American Society for Testing and Materials, 1975, pp. 364-377.

7. Hyer, M.W., Maas, L.C., and Fuchs, H.P., "The Effect of Layer Waviness on the Stress State in Hydrostatically Loaded Cylinders," Technical Report No. 87-12, Department of Mechanical Engineering, University of Maryland, College Park, Md. 20742.

8. Ramkumar, R.L., Grimes, G.C., Adams, D.F., and Dusablon, E.G., "Effects of Materials and Processes Defects on the Compression Properties of Advanced Composites," Northrop Technical Report NOR-82-103, May 1982.

9. Camponeschi, E.T., Jr., "Compression Testing of Thick-Section Composite Materials," David Taylor Research Center Technical Report SME-89-73, October 1989.

10. "Environmental Effects on Advanced Composite Materials," ASTM Special Technical Publication, No. 602, ASTM, 1976.

11. "Advanced Composite Materials-Environmental Effects," ASTM STP 658, ASTM, 1978.

12. Grant, T.S. and Bradley, W.L., "Salt Water Degradation of Polymeric Composites," Proceedings of the 9th International Conference on Offshore Mechanics and Arctic Engineering, Vol. III, February 18-23, 1990.

13. ASTM Specification D-3410-87, ASTM Book of Standards, Vol. 15.03, 1989.

14. Lamothe, K.M. and Nunes, J., "Evaluation of Fixturing for Compression Testing of Metal Matrix and Polymer/Epoxy Composites," Compression Testing of Homogeneous Materials and Composites, ASTM STP 808, Richard Chait and Ralph Papirno, Eds., American Society for Testing and Materials, 1983, pp. 241-253.

15. Adsit, N.R., "Compression Testing of Graphite/Epoxy," Compresion Testing of Homogeneous Materials and Composites, ASTM STP 808, Richard Chait and Ralph Papirno, Eds., American Society for Testing and Materials, 1983, pp. 175-186.

16. Clark, R. and Lisagor, W., "Compression Testing of Graphite/Epoxy Composite Materials," Test Methods and Design Allowables for Fibrous Composites, ASTM STP 734, C.C. Chamis, Ed., ASTM, 1981.

17. Bogetti, T., Gillespie, J., and Pipes, R.B., "Evaluation of the IITRI Compression Test Method for Stiffness and Strength Determination," University of Delaware Report CCM-87-09, March 1987.

18. Shuart, M.J., "An Evaluation of the Sandwich Beam Compression Test Method for Composites," ASTM STP 734, ASTM, 1981.

19. Cyanimid Data Sheet for FM-123 Adhesive.

20. ASTM Specification D-695-84, ASTM Book of Standards, Vol 08.01, 1985.

21. Barker, A.J. and Balasundaram, V., "Compression Testing of Carbon Fibre-Reinforced Plastics Exposed to Humid Environments," Composites, Vol. 18, No. 3, July 1987, pp. 217-225.

22. Shuart, M.J., "Failure of Compression Loaded Multi-Directional Composite Laminates," AIAA Paper No. 88-2293, April 1988.

23. Smoot, M.A., "Compressive Response of Hercules AS4/3501-6 Graphite/Epoxy Composites," University of Delaware Report CCM-82-16, June 1982.

24. Greszczuk, L.B., "Failure Mechanisms of Composites Subjected to Compression Loading," Report No. AFML-TR-72-107, August 1972.

25. Garala, H.J., "Experimental Evaluation of Graphite/Epoxy Composite Cylinders Subjected to External Hydrostatic Compressive Loading," Proceedings of the 1987 Spring Conference on Experimental Mechanics, Society for Experimental Mechanics, pp. 948-951 (1987).

26. Hom, K., Buhl, J.E., and Couch, W.P., "Hydrostatic Pressure Tests of Unstiffened and Ring-Stiffened Cylindrical Shells Fabricated of Glass-Filament Reinforced Plastics," David Taylor Model Basin Report 1745, September 1963.

27. Dally, J., Nelson, H.R., and Cornish, R.H., "Fatigue and Creep Properties of Glass-Reinforced Plastics Under Compressive States of Stress," ASME Paper 63-WA-236, September 1963.

28. Camponeschi, E.T., Jr., "Compression of Composite Materials: A Review," DTRC TR 87-050, November 1987.

29. Rosen, B.W., "Mechanics of Composite Strengthening," Fiber Composite Materials, ASM, 1964.

30. Greszczuk, L.B., "Microbuckling Failure of Circular Fiber-Reinforced Composites," AIAA Journal, Vol. 13, No. 10, Oct. 1975, pp. 1311-1318.

31. Sadowsky, M.A., Pu, S.L., and Hussain, M.A., "Buckling of Microfibers," Journal of Applied Mechanics, Vol. 34, December 1967, pp. 1011-1016.

32. Herrmann, L.R., Mason, W.E., and Chan, S.T.K., "Behavior of Compressively Loaded Reinforcing Wires," Structural Engineering Laboratory Report 67-2, January

1967, University of California, Berkeley.

33. Davis, J.G., "Compressive Strength of Lamina Reinforced and Fiber Reinforced Composite Materials," PhD Thesis, Virginia Polytechnic Institute and State University, Blacksburg, Va., May 1973.

34. Budiansky, B., "Micromechanics," Computers and Structures, Vol. 16, No. 1-4, 1983, pp. 6-10.

35. Sinclair, J.H. and Chamis, C.C., "Compressive Behavior of Unidirectional Fibrous Composites," Compression Testing of Homogeneous Materials and Composites, ASTM STP 808, Chait and Papirno, Eds., ASTM, 1983.

36. Piggott, M.R., "A Theoretical Framework for the Compressive Properties of Aligned Fiber Composites," Journal of Materials Science, 16, 1981.

37. Shuart, M.J., "Short Wavelength Buckling and Shear Failures for Compression-Loaded Composite Laminates," NASA TM-87640, November 1985.

38. Environmental Effects on Composite Materials. George Springer, Ed., Technomic Publishing Co., 1981.

39. Tsai,S., "Environmental Factors in the Design of Composite Materials," in Composite Materials Workshop, edited by S.W. Tsai, J.C. Halpin, and N.J. Pagano, Technomic Publishing Co., Inc., Stanford, Conn., 1968, pp. 749-767.

40. Weitsman, Y., "Coupled Damage and Moisture Transport in Fiber-Reinforced Polymeric Composites," Int. Journal Solids Structures, Vol. 23, No. 7, 1987, pp. 1003-1025.

41. Adams, D.F. and Monib, M.M., "Moisture Expansion Coefficients ofa Polymer Matrix Composite Material," Proceedings of the Fourth Conference on Fibrous Composites in Structural Design, Army Materials and Mechanics Research Center, Watertown, Mass., November 1978.

42. Browning, C.E., Husman, G.E. and Whitney, J.M., "Moisture Effects in Epoxy Matrix Composites," Composite Materials: Testing and Design (Fourth Conference) ASTM STP 617, American Society of Testing and Materials, 1977, pp. 481-496.

43. Snead, J.M. and Palazotto, A.N., "Moisture and Temperature Effects on the Instability of Cylindrical

Composite Panels," AIAA, Journal of Aircraft, 20, September 1983, pp. 777-783.

44. Straw, Anthony D., "The Buckling of Composite Cylindrical Panels Considering Environmental Effects," AFIT/GAE/AA/85D-15, December 1985.

45. Jost, W., Diffusion in Solids, Liquids, and Gases. Academic Press (1960).

46. Shirrell,C. and Sandow, F.A., "The Kinetics of Moisture Diffusion in Three Advanced Composite Epoxy Resin Matrix Material Systems," in Fibrous Composites in Structural Design, Nov. 14-17,1987, San Diego, Lenoe et al, Eds., pp. 795-808.

47. Collings, T.A. and Copley, S.M., "On the Accelerated Ageing of CFRP," Composites, Vol. 14, No. 3, July 1983, pp. 180-188.

48. Farrer, N.R. and Ashbee, K.H.G., "Self-Stress Enhanced Water Migration in Composites," Org. Coat. Plast. Chem., Vol. 40, 1979, pp. 947-953.

49. Course notes from Micromechanical Analysis of Composite Materials: Applications to Practical Problems" taught by Professor D. Adams from the University of Wyoming.

50. Grimes, G.C., "Experimental Study of Compression-Compression Fatigue of Graphite/Epoxy Composites," Test Methods and Design Allowables for Fibrous Composites, ASTM STP 734, C.C. Chamis, Ed., American Society for Testing and Materials, 1981, pp. 281-337.

51. Grimes, G.C. and Adams, D.F., "Investigation of Compression Fatigue Properties of Advanced Composites," Northrop Report No. NOR-79-17.

52. Ramani, S.V. and Nelson, H.G., "Effect of Moisture on the Fatigue Behavior of Graphite/Epoxy Composite Laminates," Report No. NASA-TM-78548, A-7689, January 1979.

53. ASTM Specification D-3171-76, ASTM Book of Standards, Vol. 15.03, 1989.

54. Hercules Data Sheet for 3501-6 epoxy resin.

55. Verbal Communication with Prof. Don Adams, University of Wyoming, February 1990.

56. Dally, J.W., Riley, W.F., and McConnell, K.G., Instrumentation for Engineering Measurements, John Wiley and Sons, Inc., New York, 1984.

57. ABAQUS User's Manual, Version 4.7, written by Hibbitt, Karlsson, and Sorensen.

58. Hyer, M.W., "Response of Thick Laminated Cylinders to External Hydrostatic Pressure," University of Maryland Technical Report No. 87-4, May 1987.

59. Camponeschi, E.T., "Through-Thickness Strain Response of Thick Composites in Compression," DTRC TR 89-067, September 1989.

60. Chi-Hung, S., and Springer, G.S., "Environmental Effects on the Elastic Moduli of Composite Materials," Journal of Composite Materials, Vol. 11, July 1977, pp. 250-264.

61. Tretheway, Bruce Jr., Wilkens, Dick J., and Gillespie, John W. Jr., "Three-Dimensional Elastic Properties of Laminated Composites," CCM Report 89-04, University of Delaware (1989).

62. Pagano, N.J., "Exact Moduli of Anisotropic Laminates,"Mechanics of Composite Materials, Sendeckyi,Ed., Academic Press, 1984, pp. 23-44.

63. Tsai, Stephen W. and Hahn, H. Thomas, Introduction to Composite Materials, Technomic Publishing Co., Westport, Connecticut, 1980.

64. Camponeschi, E.T., "Compression Response of Thick-Section Composite Materials," PhD Thesis, University of Delaware, August 1990.

65. Telegadas, H.K. and Hyer, M.W., "The Influence of Layer Waviness on the Stress State in Hydrostatically Loaded Cylinders: Further Results," CCMS-89-22, Virginia 1989.

66. Jones, R.M., Mechanics of Composite Materials, McGraw-Hill Book Co., New York, 1975.

67. Handbook of Composites, Ed. George Lubin, New York: Van Nostrand Reinhold Co., 1982.

68. Timoshenko, S.P. and Gere, J.M., Theory of Elastic Stability, McGraw-Hill, New York (1961) Polytechnic Institute and State University Report, November 1989.

Table 1 Elastic Constants
for
AS4 Fiber

Elastic Constants	AS4 Fiber GPa (psi)
E1	237 (34E6)
E2	14 (2E6)
E3	14 (2E6)
ν_{12}	.20
ν_{13}	.30
ν_{23}	.30
G12	14 (2E6)
G13	14 (2E6)
G23	5 (.77E6)

Fiber Radius 7E-6 m (2.76E-4 in.)

Table 2 Elastic Constants
for
3501-6 Resin

Elastic Constants	3501-6 Resin GPa (psi)
E	4 (.62E6)
v	.34
G	1.6 (.23E6)

Table 3 Compression Strength for Thick (6.35 mm) AS4/3501-6 $(0_2/90)_s$ Composites

Specimen Number	DRY Compression Strength MPa (ksi)	WET Compression Strength MPa (ksi)
1	1048 (150)	740 (106)
2	1006 (144)	761 (109)
3	1118 (160)	796 (114)
4	1027 (147)	838 (120)
5	1048 (150)	733(105)
6	1013 (145)	796 (114)
7	1083 (155)	796 (114)
8	1069 (153)	684 (98)
9	1020 (146)	656 (94)
10	1076 (154)	601 (86)
11	1104 (158)	----
12	1020 (146)	----
13	1055 (151)	----
14	1076 (154)	----
15	1027 (147)	----
Mean	1055(151)	740(106)
S_x	36(5.2)	72(10.3)
$S_{\bar{x}}$	9(1.34)	23(3.2)
$t(\alpha)S_{\bar{x}}$	19(3)	52(7)

S_x Standard Deviation

$S_{\bar{x}}$ Standard Deviation of the Mean

$t(\alpha)$ Student's t Statistic

Table 4 Compression Strength for Thin (1.6 mm) AS4/3501-6 (0_2/90)$_s$ Composites

Specimen Number	DRY Compression Strength MPa (ksi)	WET Compression Strength MPa (ksi)
1	1002(143.5)	796(114)
2	1006(144)	1076(154)
3	1132(162)	803(115)
4	1059(151.6)	1135(162)
5	1002(143.5)	789(113)
6	964(138)	1111(159)
7	1166(167)	908(130)
8	1257(180)	1132(162)
9	1139(163)	803(115)
10	1145(164)	733(105)
11	----	1071(153)
12	----	845(121)
13	----	950(136)
14	----	873(125)
15	----	1118(160)
16	----	1111(159)
17	----	1062(152)
Mean	1087(155.7)	957(137)
S_x	94(13.5)	147(21)
$S_{\bar{x}}$	30(4.3)	36(5)
$t(\alpha)S_{\bar{x}}$	68(9.7)	75(11)

S_x Standard Deviation

$S_{\bar{x}}$ Standard Deviation of the Mean

$t(\alpha)$ Student's t Statistic

Table 5 Elastic Constants for Dry and Wet (Saturated, Room Temperature) AS4/3501-6 Laminates $V_F = 60\%$

	Unidirectional		$(0_2/90)_s$ Laminate	
	Dry GPa (psi)	Wet GPa (psi)	Dry GPa (psi)	Wet GPa (psi)
E11	117(16.7E6)	117(16.7E6)	82(11.7E6)	81(11.6E6)
E22	10(1.5E6)	9.2(1.3E6)	46(6.6E6)	45(6.5E6)
E33	10(1.5E6)	9.2(1.3E6)	12(1.8E6)	10(1.5E6)
v12	.33	.33	.075	.067
v13	.33	.33	.451	.455
v23	.47	.47	.47	.47
G12	6(.87E6)	6(.87E6)	6(.87E6)	6(.87E6)
G13	6(.87E6)	6(.87E6)	5(.73E6)	5(.73E6)
G23	3.8(.55E6)	3.8(.55E6)	4.4(.63E6)	4.4(.63E6)

1 Fiber Direction
2 Transverse to Fiber
3 Through Thickness

1 0° Direction
2 90° Direction
3 Trhough Thickness

Table 6 Maximum Matrix Shear Stresses Due to Axial Compressive Loads In An Initailly Wavy AS4/3501-6 Ply

		Maximum Matrix Shear Stress MPa (ksi)	
a/L	G_m^* GPa(Msi)	1.2%Strain	1.5% Strain
0.00375	1.60(0.23)	———	65.0(9.3)
	0.99(0.14)	44.0(6.2)	54.0(7.8)
	0.37(0.05)	———	34.0(4.8)
0.009	1.60(0.23)	———	140.0(20.0)
	0.99(0.14)	91.0(13.0)	112.0(16.0)
	0.37(0.05)	———	68.0(9.7)

*Value of matrix shear modulus used in finite element analysis

Table 7 Comparison of Predicted and Measured Compression Strengths

	V_F	V_M	G_F GPa(Msi)	G^*_{MT} MPa(Msi)	σ_{uni} MPa(ksi)	Predicted $\sigma_{0_2/90}$ MPa(ksi)	Measured $\sigma_{0_2/90}$ MPa(ksi)
Dry Thick	.62	.38	14(2)	1187(.17) 629(.09)	2717(389) 1544(221)	1837(263) 1048(150)	1055(151) 1055(151)
Wet Thick	.62	.38	14(2)	978(.14) 419(.06)	2291(328) 1055(151)	1551(222) 712(102)	740(106) 740(106)
Dry Thin	.66	.34	14(2)	1187(.17) 629(.09)	2969(425) 1697(243)	2005(287) 1153(165)	1090(156) 1090(156)
Wet Thin	.66	.34	14(2)	1048(.15) 489(.07)	2689(385) 1348(193)	1816(260) 908(130)	957(137) 957(137)

* Matrix tangent shear modulus corresponding to appropriate matrix shear stress from analysis

Figure 1 Celanese Compression Fixture
Copyright ASTM. Reprinted with permission.

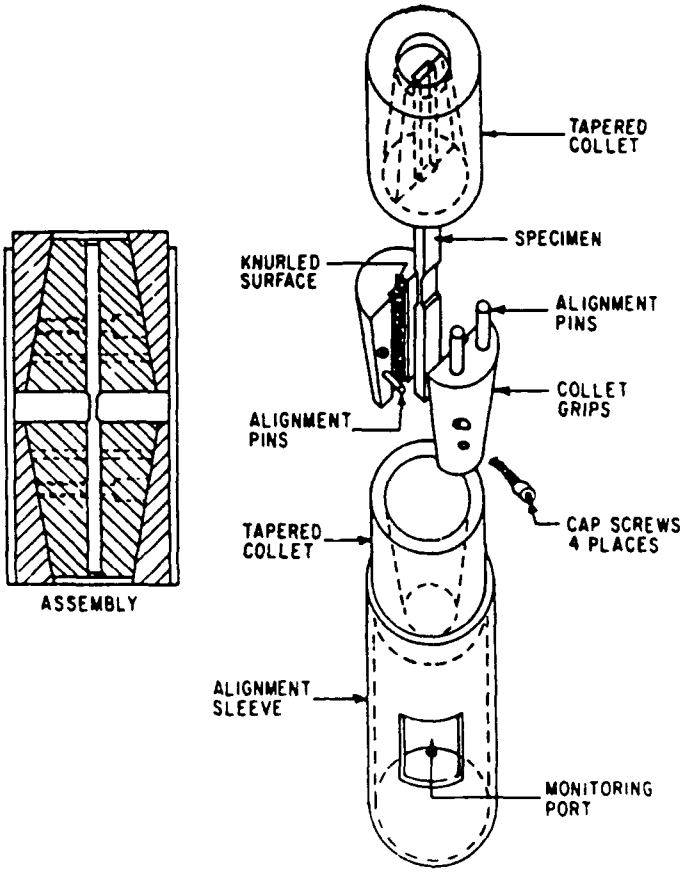

Figure 2 IITRI Compression Fixture
Copyright ASTM. Reprinted with permission.

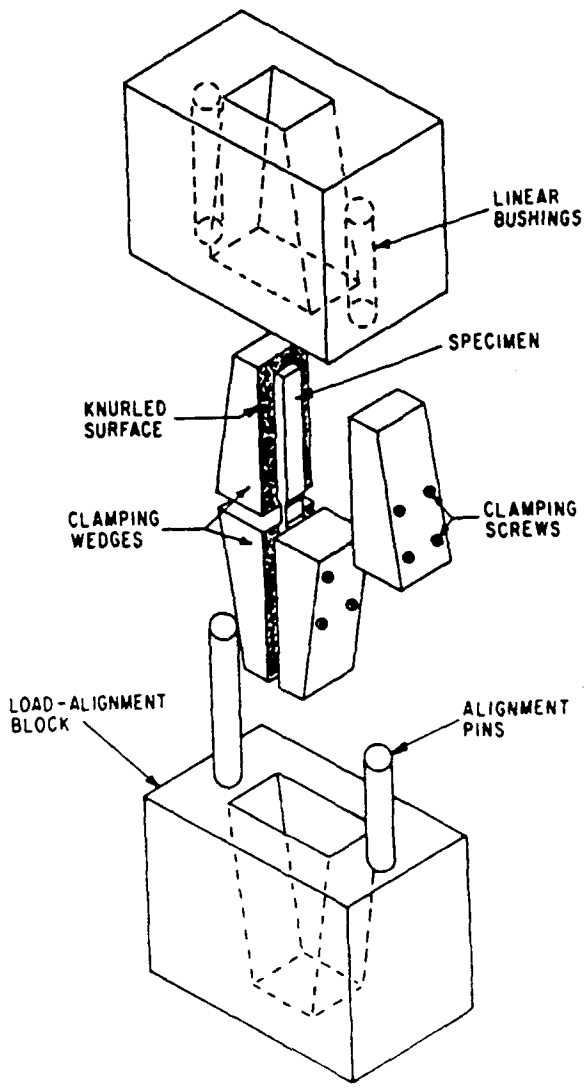

Figure 3 Sandwich Beam Test Specimen
Copyright ASTM. Reprinted with permission.

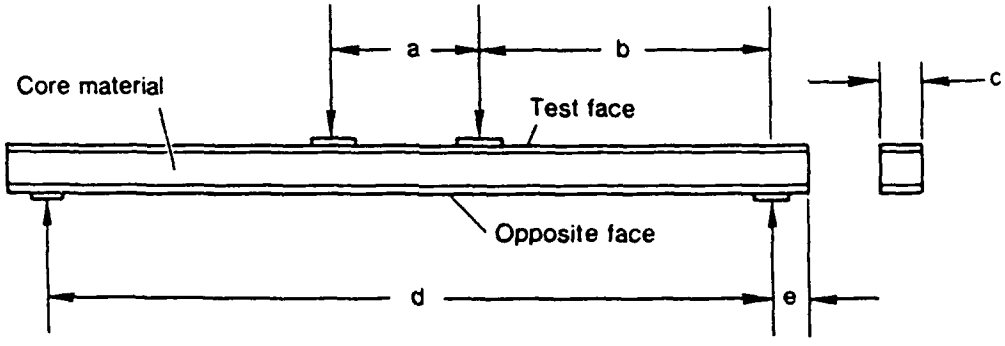

Notes.
1. Load pads — f wide
2. Reaction pads — g wide

	British system, in.	Metric, mm
a	4.0	101.6
b	8.0	203.2
c	1.0	25.40
d	20.0	508.0
e	1.0	25.4
f	1.0	25.4
g	1.5	38.1

Figure 4 Compression Test Method
for Rigid Plastics
ASTM D695
Copyright ASTM.
Reprinted with permission.

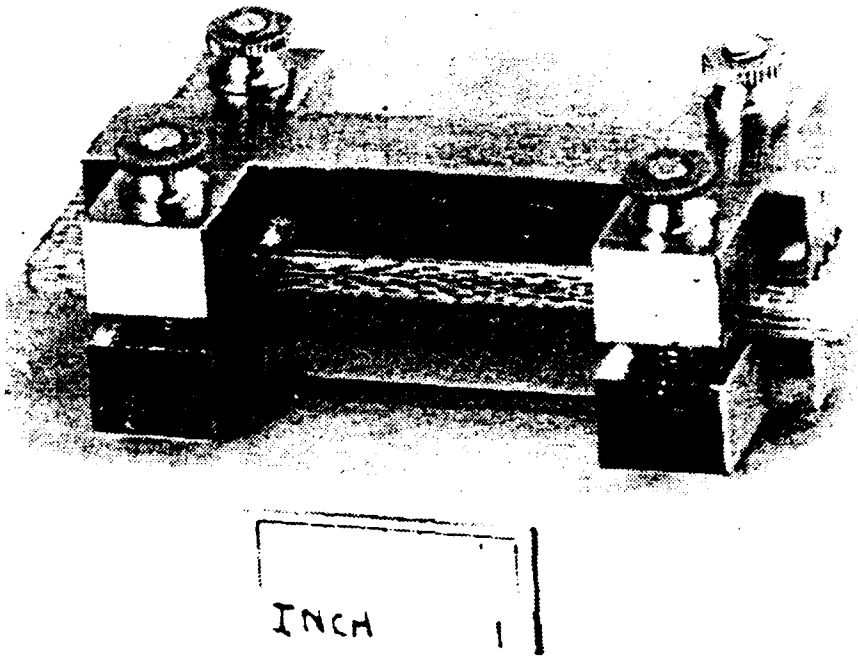

Figure 5 ASTM D695 Test Specimen Geometry
Copyright ASTM. Reprinted with permission.

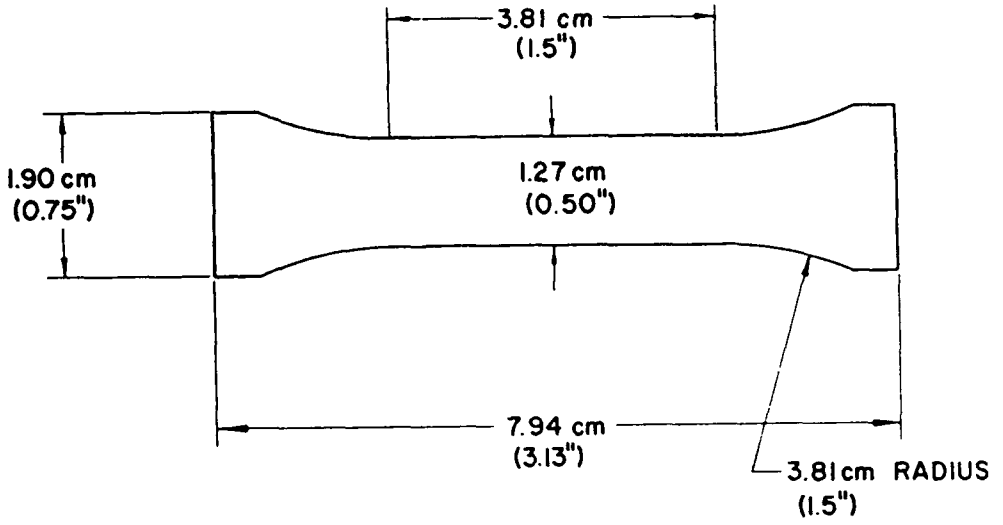

Figure 6 DTRC Compression Fixture

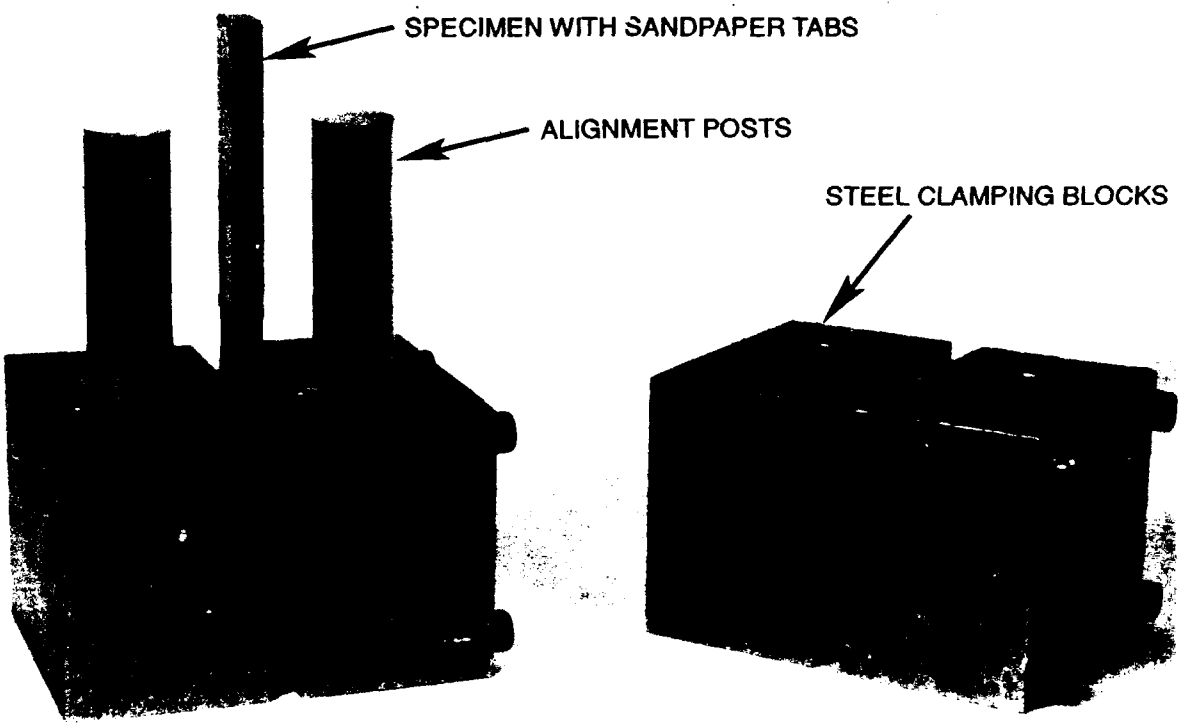

Figure 7 Failure Modes Corresponding to Highest Compression Strengths in Unidirectional AS4/3501-6 Composites Tested Using the IITRI Compression Fixture [23]

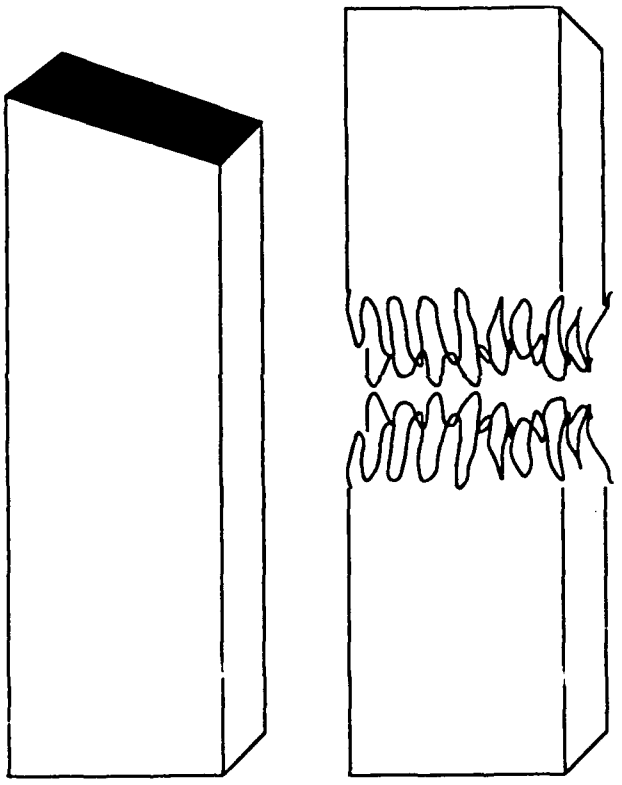

Angular Shear Across Specimen Width

Gage Section Brooming

Figure 8 Kink Band Geometry

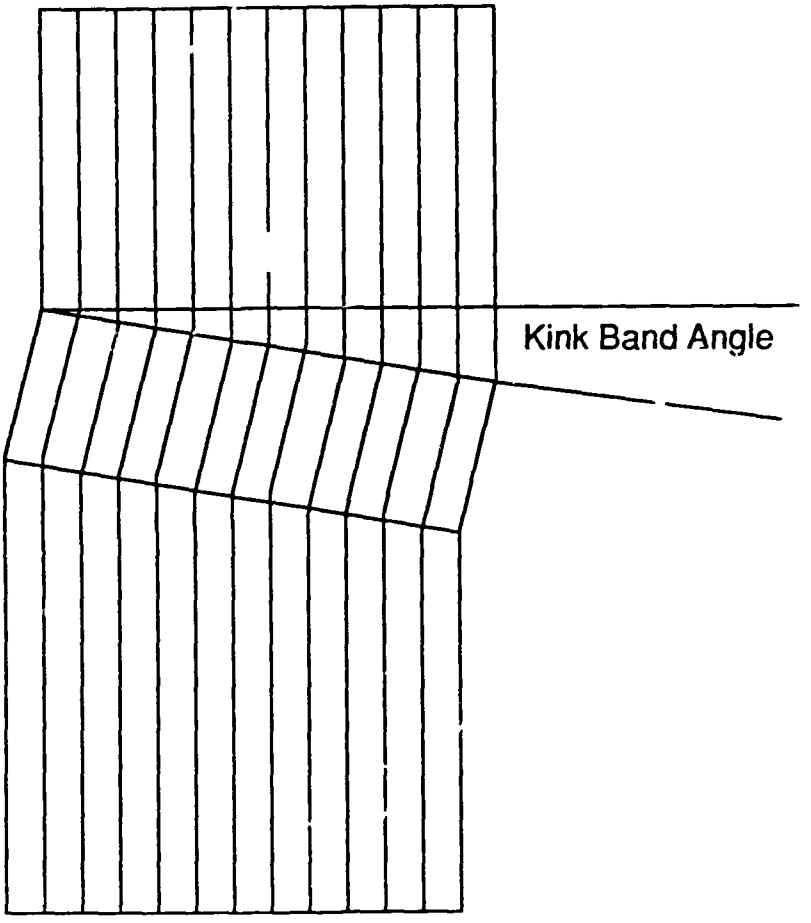

Figure 9 Boundary Conditions for Moisture Diffusion Problems

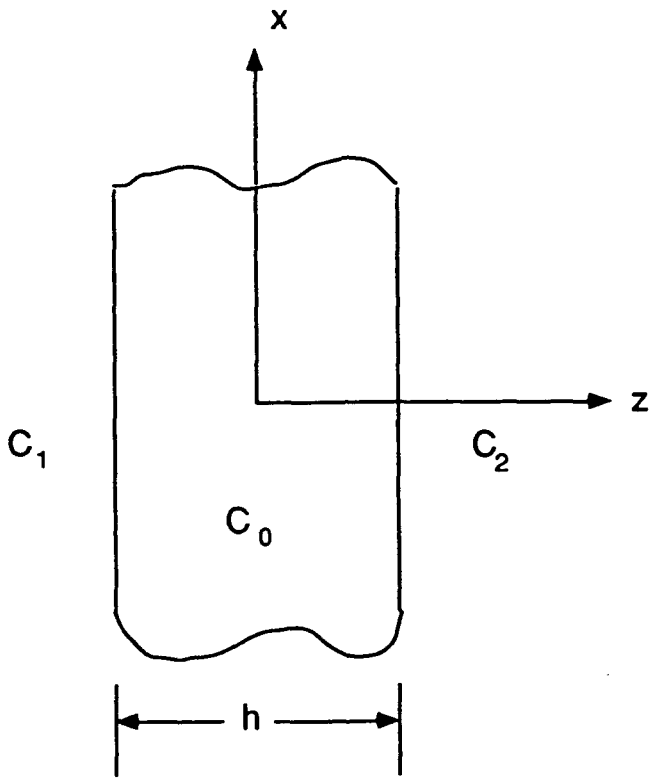

Figure 10 Orientation Angles for Calculation
Of Moisture Diffusion In A
Composite Material

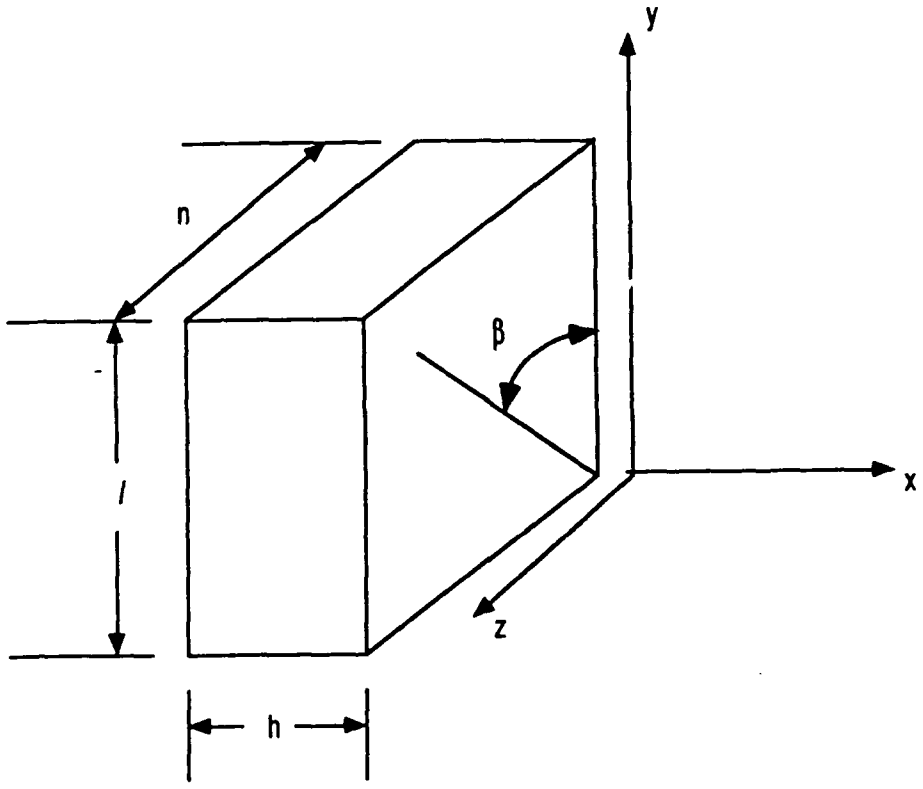

Figure 11 Curing Schedule for AS4/3501-6 Panels

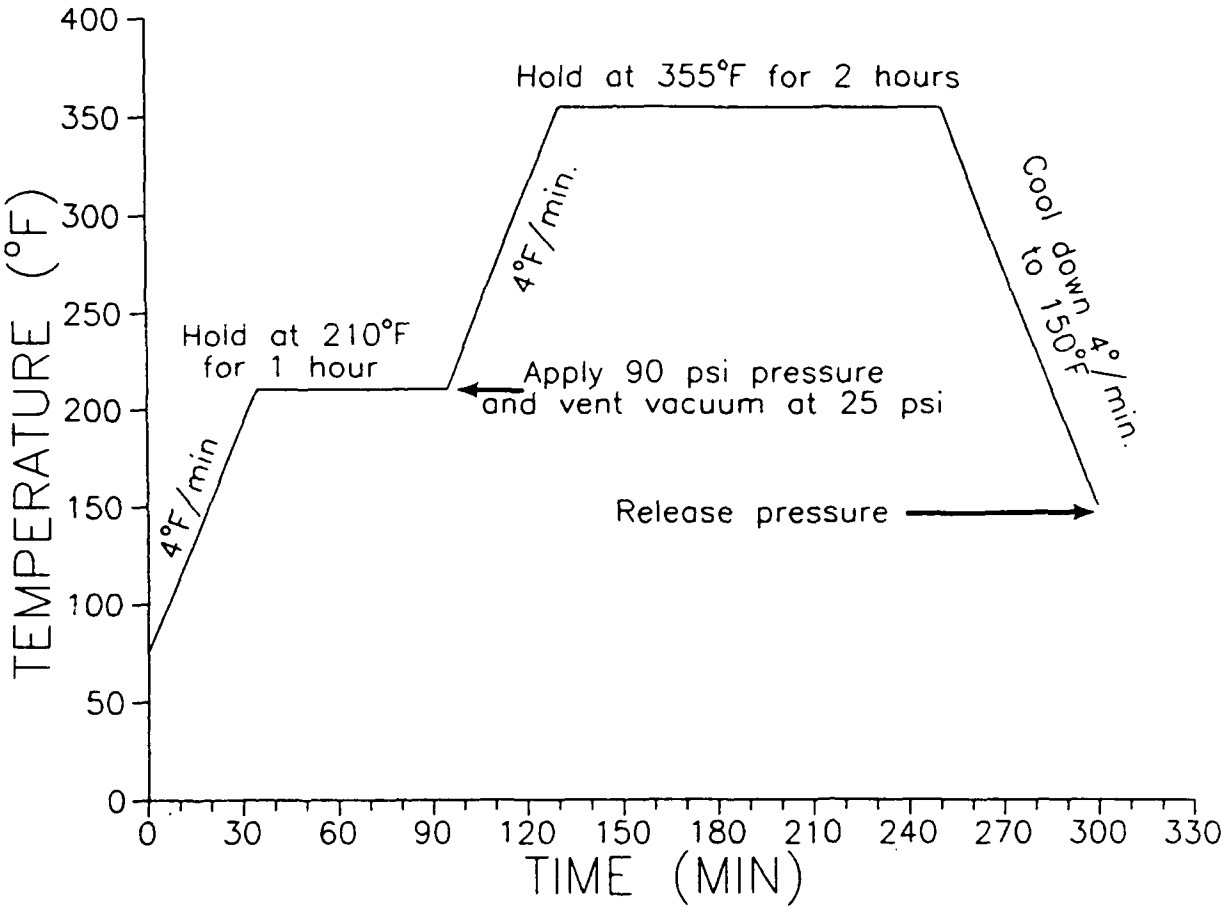

1) Apply 28 inches vacuum.
2) Heat part to 210°F at 1–5°/min.
3) Hold at 210°F for 1 hour.
4) Apply 90 psi pressure. Vent vacuum when pressure reaches 25 psi.
5) Raise temperature to 355°F at 1–5°/min.
6) Hold temperature at 355°F for 2 hours.
7) Cool to 150°F at rate of 1–5°/min.
8) Vent pressure at 150°F.
9) Hold at 355°F for 4 hours.
10) Cool to 75°F at rate of 2°/min. and vent pressure.

Figure 12 Compression Specimens

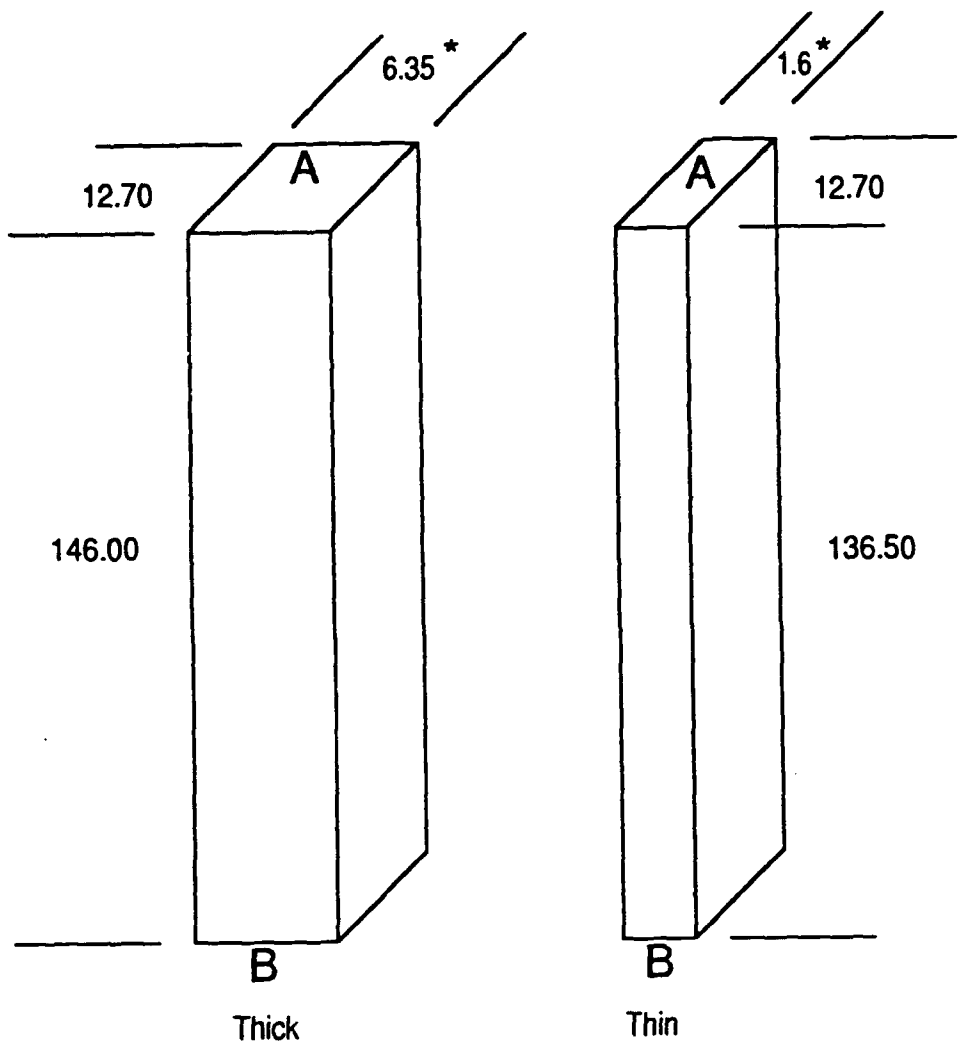

(All dimensions in millimeters)

Surfaces A and B ground flat and parallel to 0.03 mm

*Thickness as received following hand layup and autoclave cure

Figure 13 Method Used to Determine Coefficient
of Friction Between Specimen
and Fixture
With and Without Sandpaper

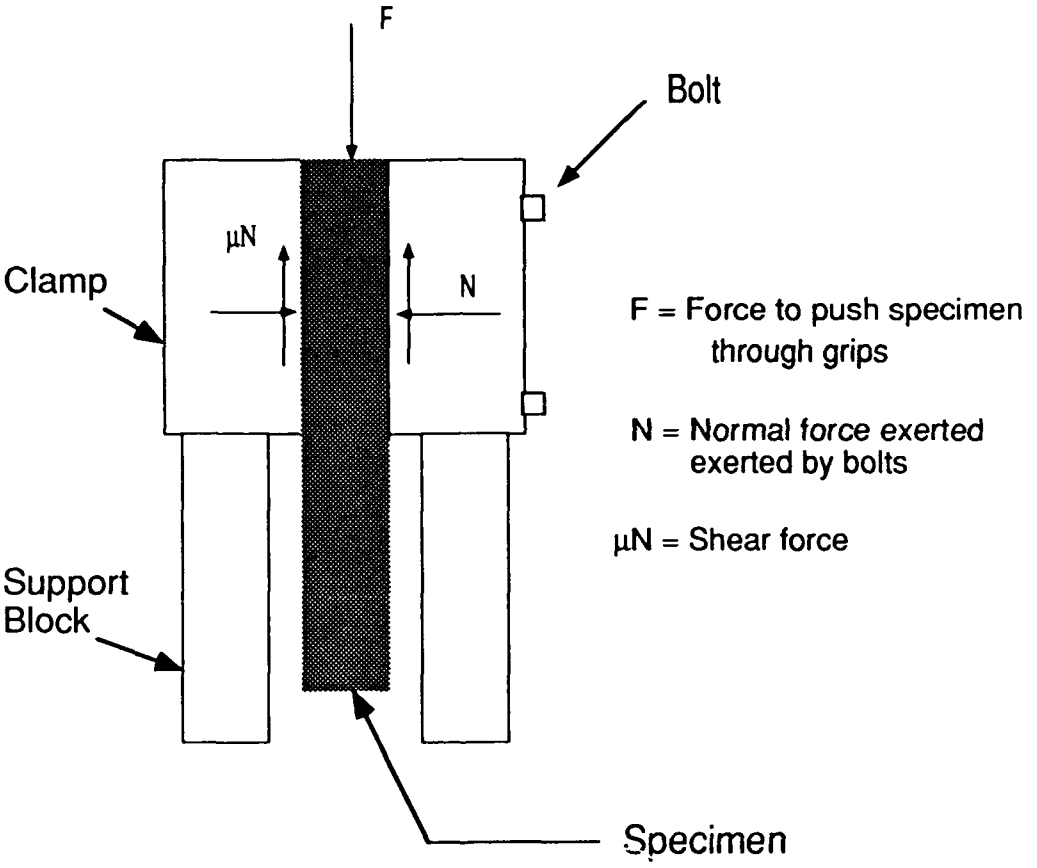

Figure 14 Elevated Temperature Setup

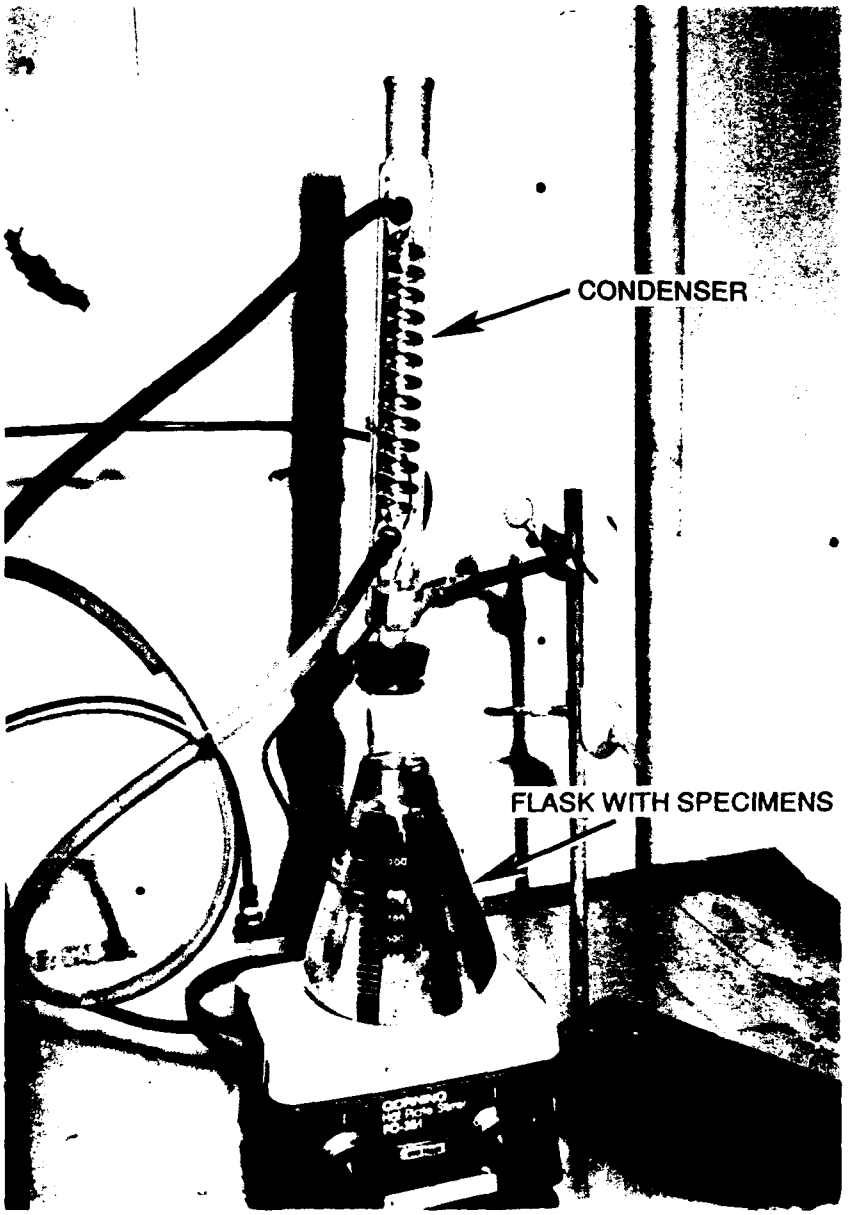

Figure 15 Schematic of DTRC Thick-Section Compression Fixture After [9]

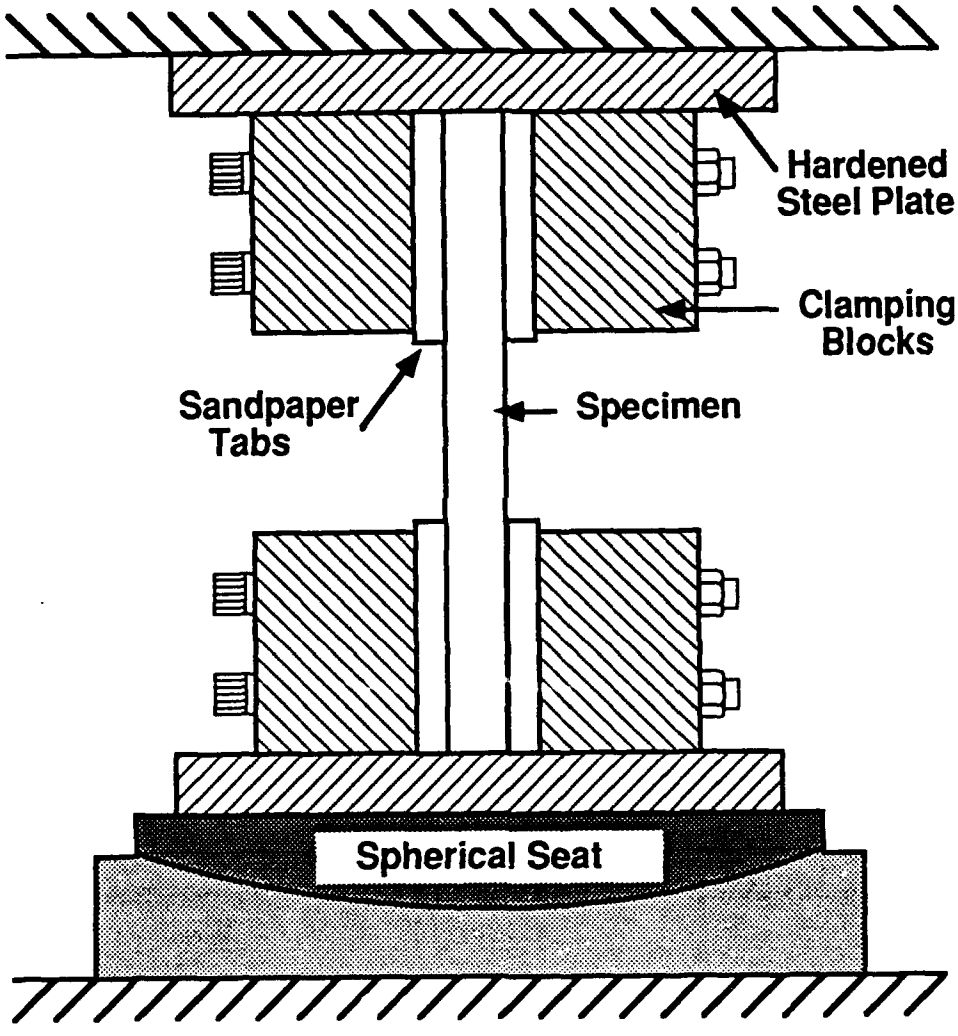

Figure 16 Compression Stress-Strain Curves
for Thick Specimens in the
Dry Condition

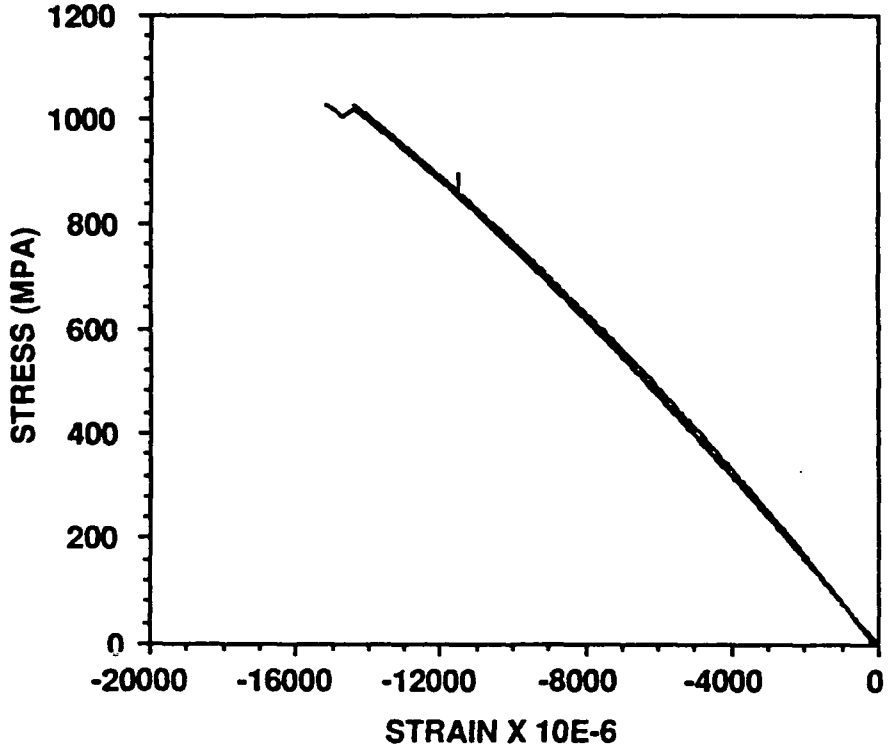

Figure 17 Compression Stress-Strain Curves
for Thick Specimens in the
Wet Condition

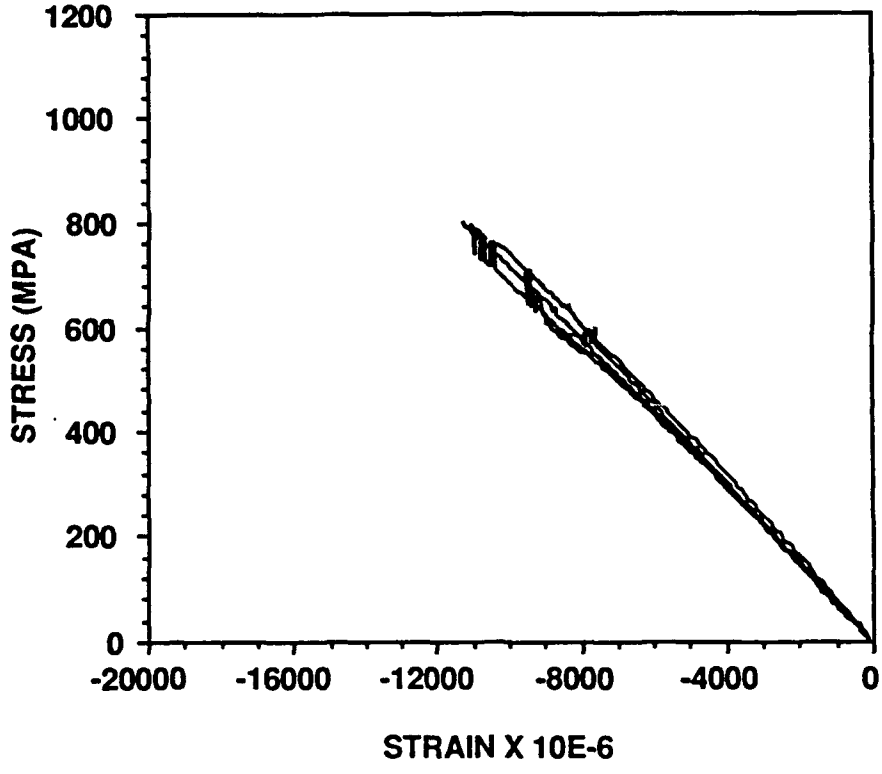

Figure 18 Compression Stress-Strain Curves
for Thin Specimens in the
Dry Condition

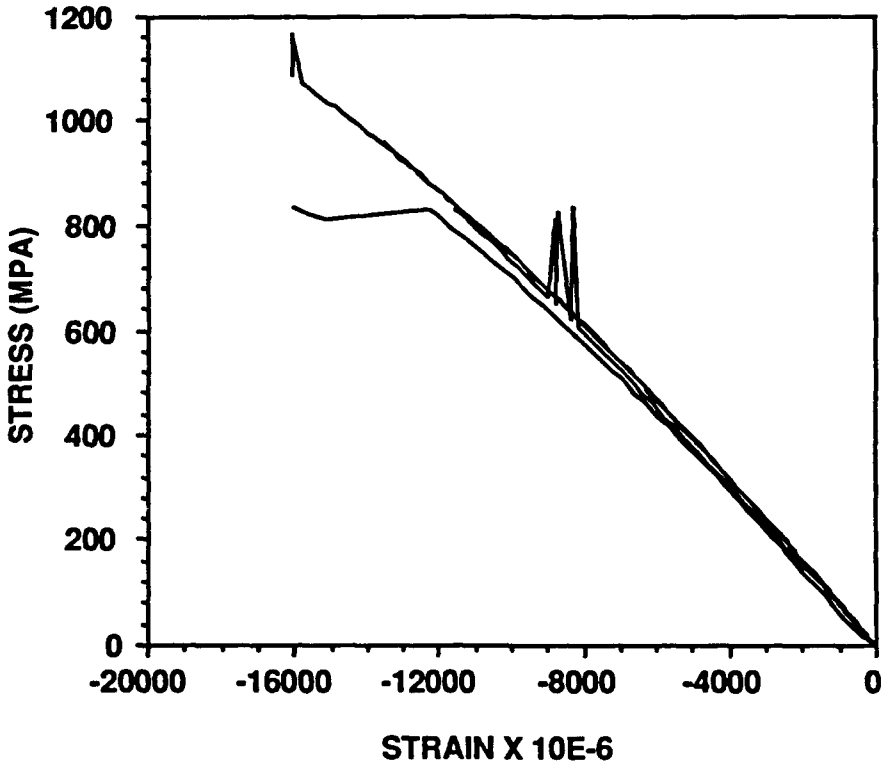

Figure 19 Compression Stress-Strain Curves
for Thin Specimens in the
Wet Condition

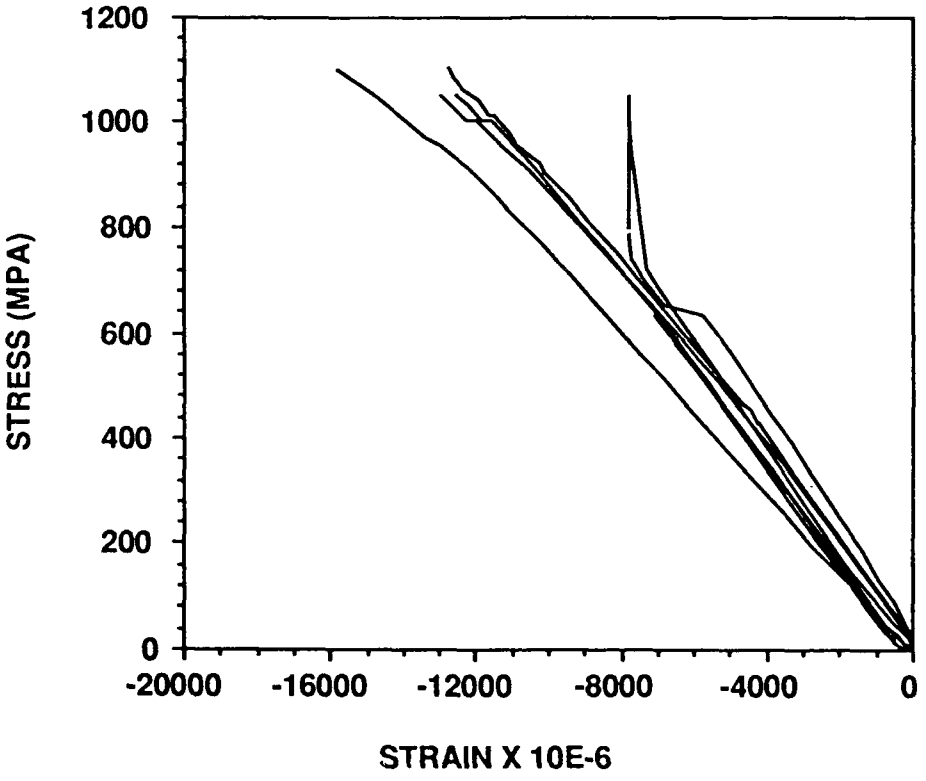

Figure 20 Typical Failure Modes for Dry and Wet AS4/3501-6 $(0_2/90)_s$ Thick (6.35 mm) Laminates

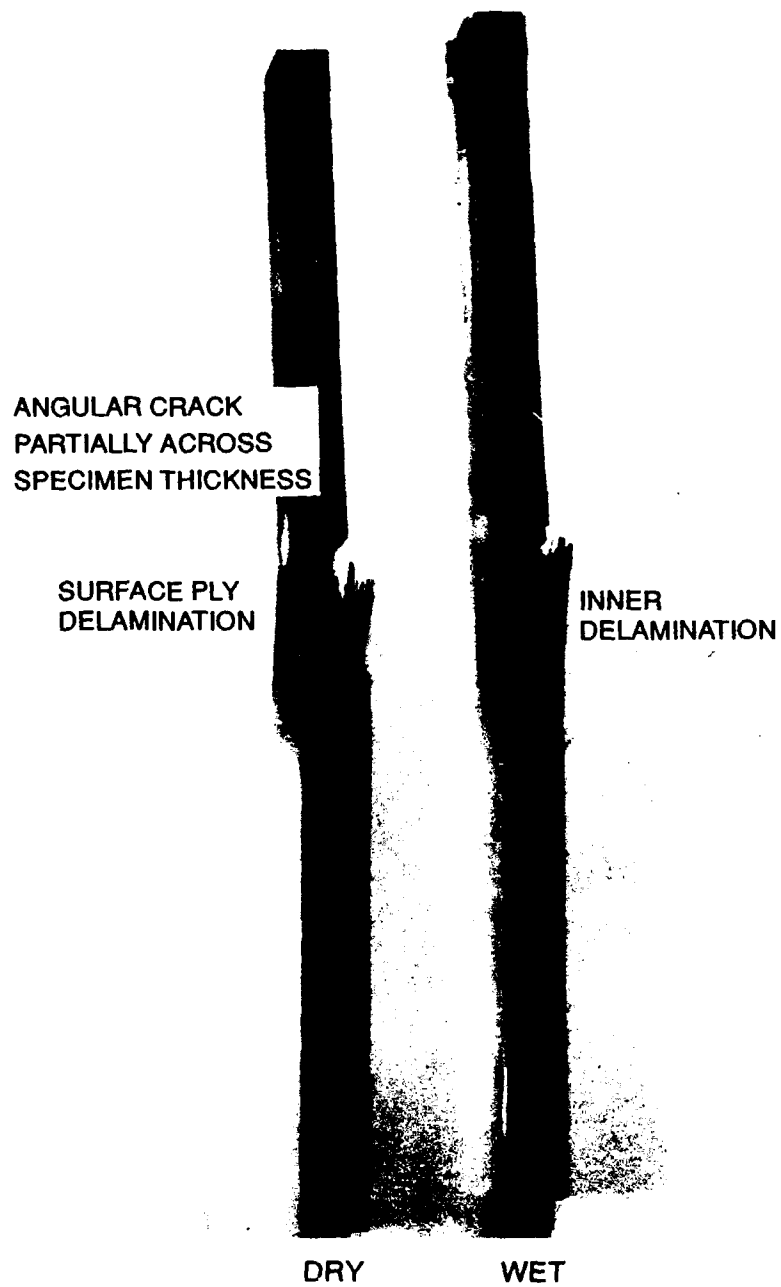

Figure 21 Typical Failure Modes for Dry and Wet AS4/3501-6 $(0_2/90)_S$ Thick (6.35 mm) Laminates Detail View of Failure Zone

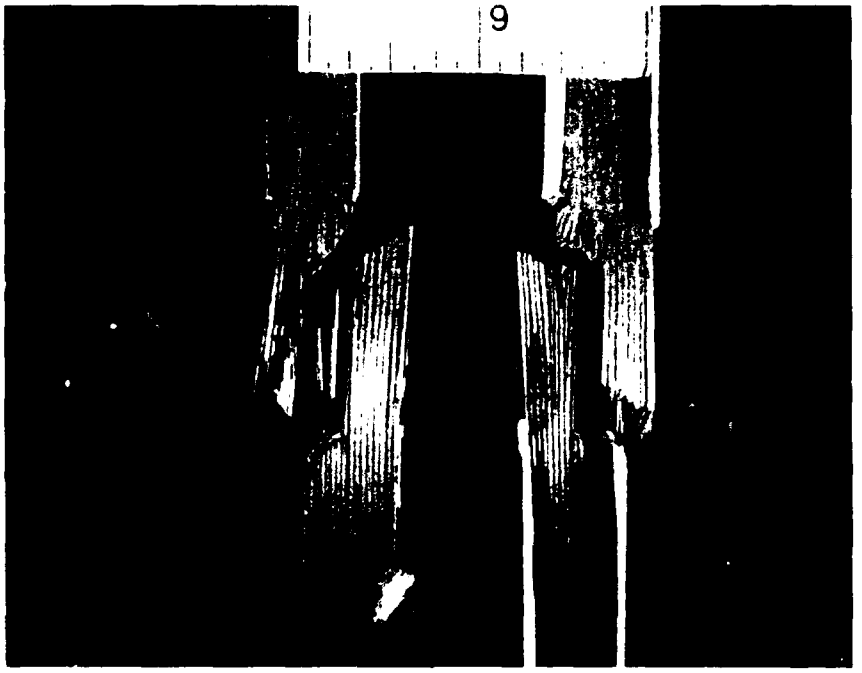

DRY WET

Figure 22 Typical Failure Modes for Dry and Wet AS4/3501-6 $(0_2/90)_S$ Thin (1.6 mm) Laminates

Figure 23 Typical Failure Modes for Dry and Wet AS4/3501-6 $(0_2/90)_S$ Thin (1.6 mm) Laminates Detail View of Failure Zone

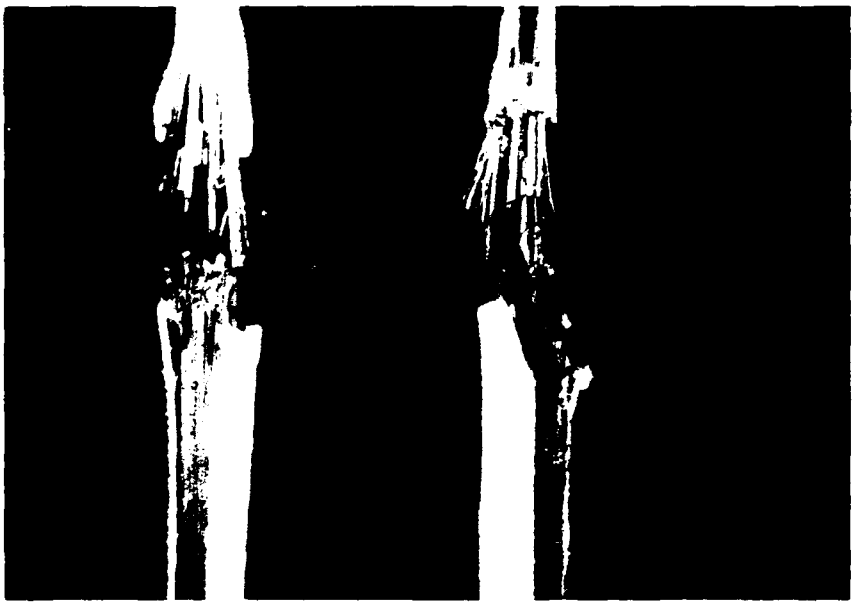

DRY WET

Figure 24 Symmetry Planes for 3-D Finite Element Analysis of Compression Specimens

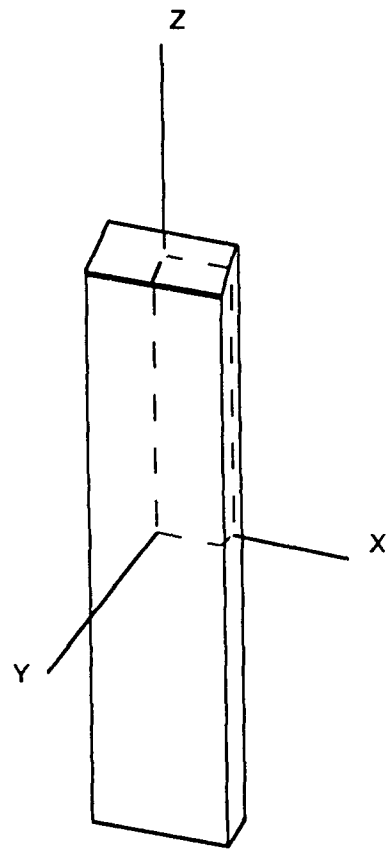

Figure 25 3-D Finite Element Model of Compression Specimen

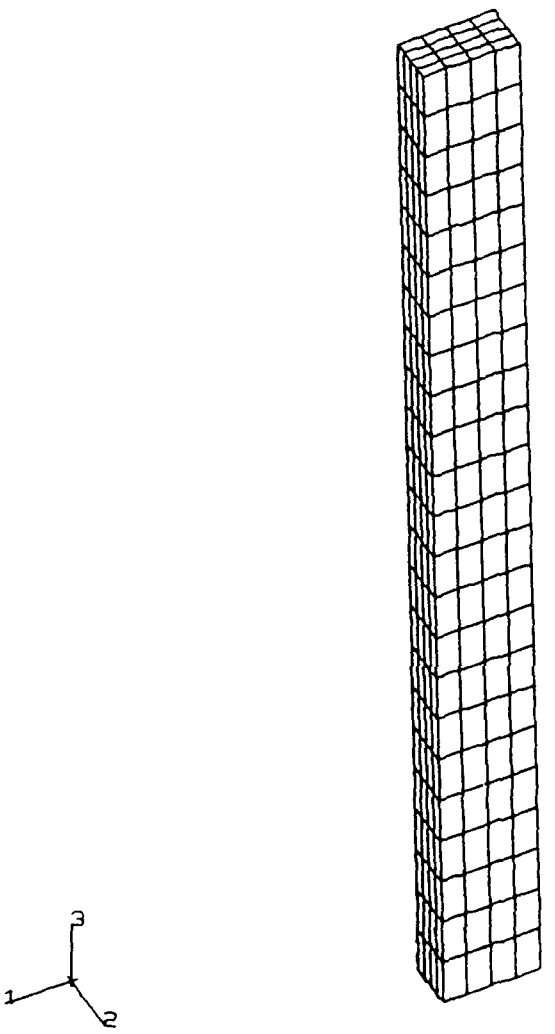

Figure 26 Boundary and Loading Conditions for 3-D Finite Element Analysis of Compression Specimens

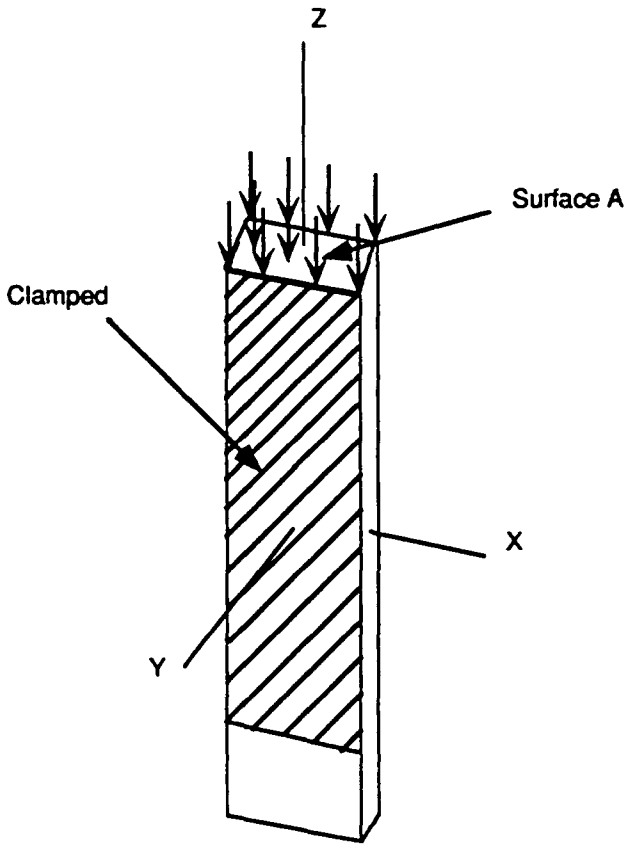

Figure 27 Distribution of Moisture Concentration Through the Thickness for Thick (6.35 mm) AS4/3501-6 $(0_2/90)_S$ Laminates

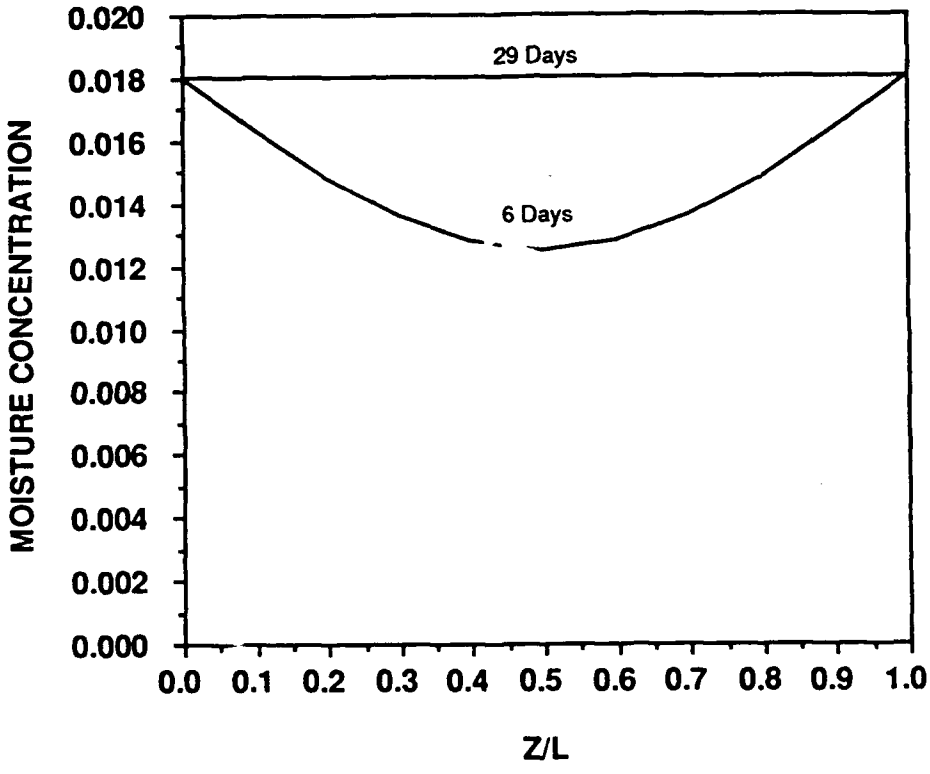

Figure 28 Distribution of Moisture Concentration Through the Thickness for Thin (1.6 mm) AS4/3501-6 $(0_2/90)_S$ Laminates

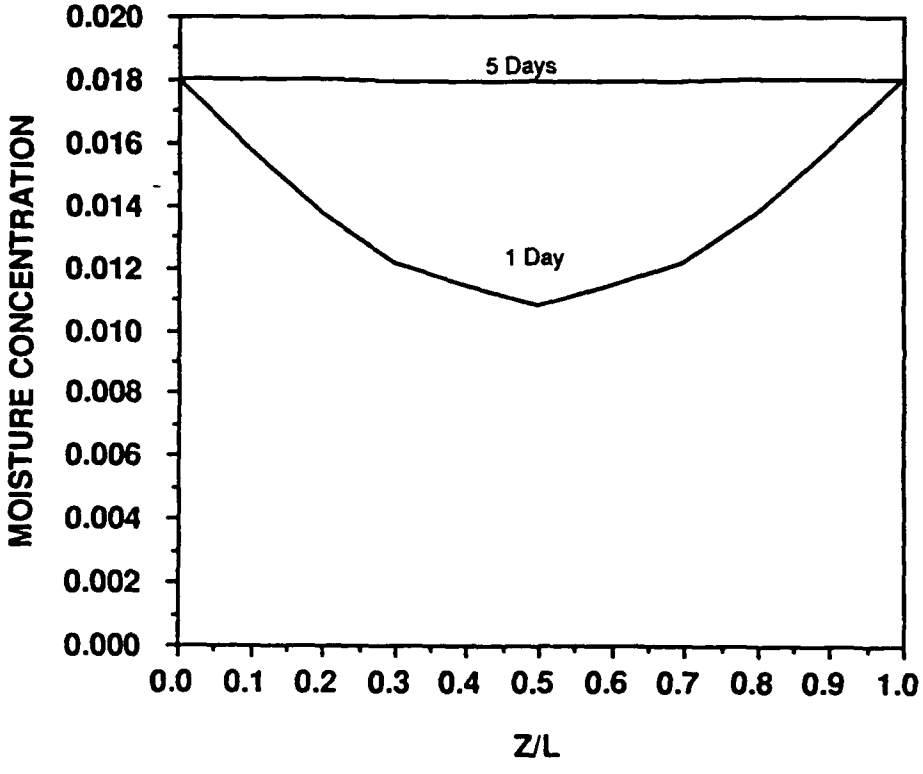

Figure 29 Micromechanical Finite Element Model of Fiber Plate and Surrounding Matirx Layers

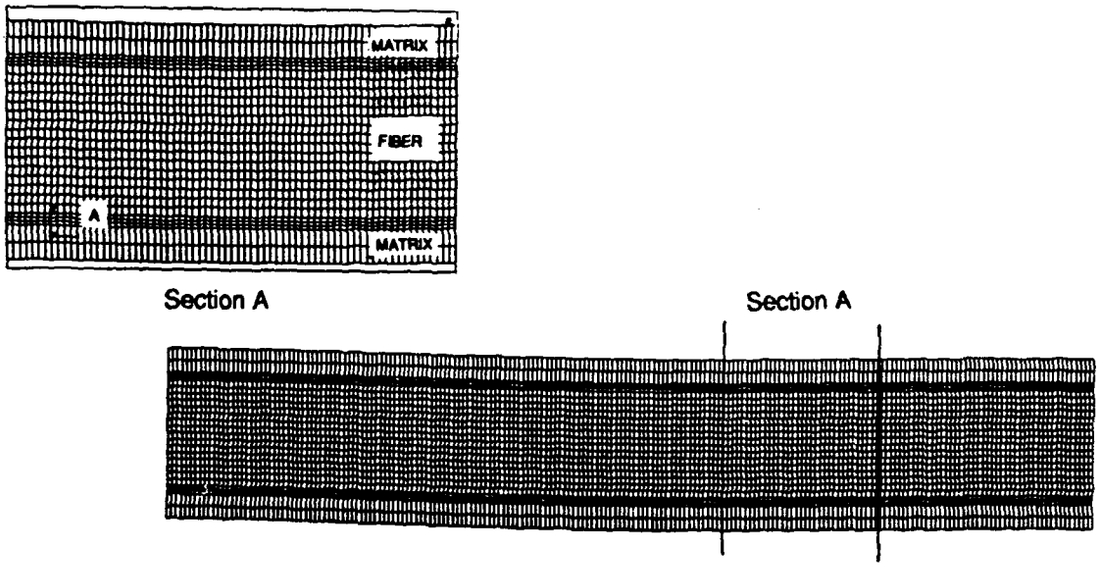

a) Single Fiber Plate Model

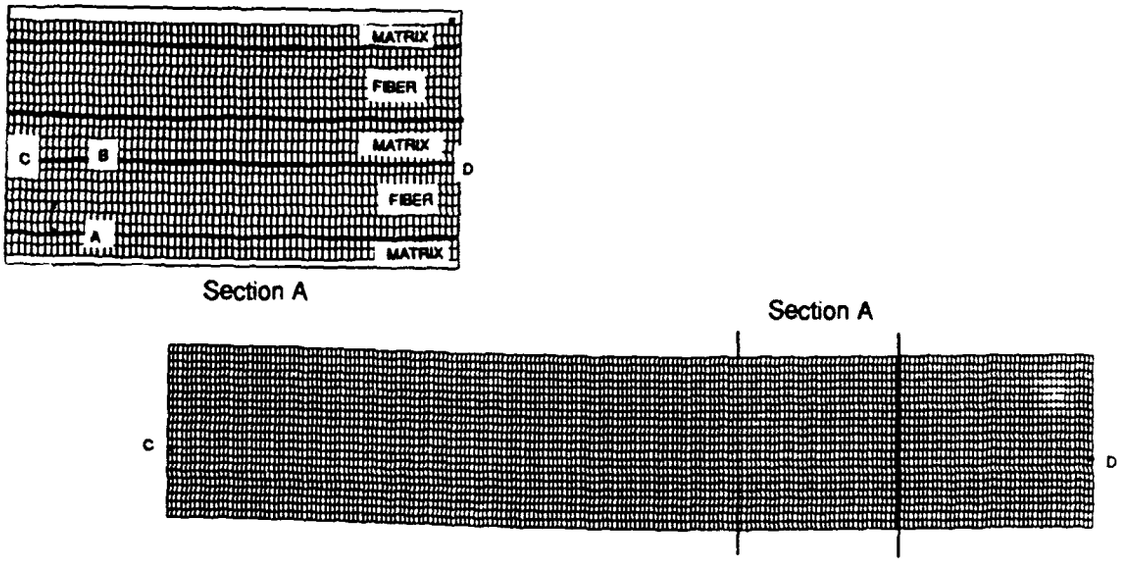

b) Double Fiber Plate Model

Figure 30 3501-6 Resin Shear Stress-Strain Curves Generated with Richard-Blacklock Shear Model

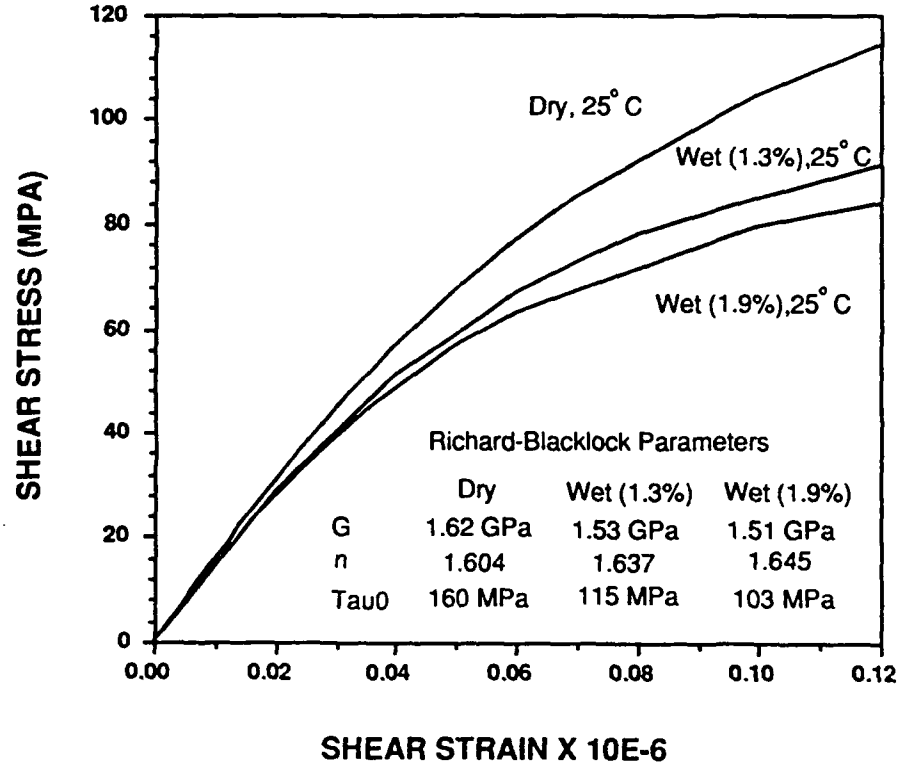

Figure 31 Rotated Shear Stresses at the Integration Points on Either Side of the Fiber-Matrix Interface a/L = 0.00375

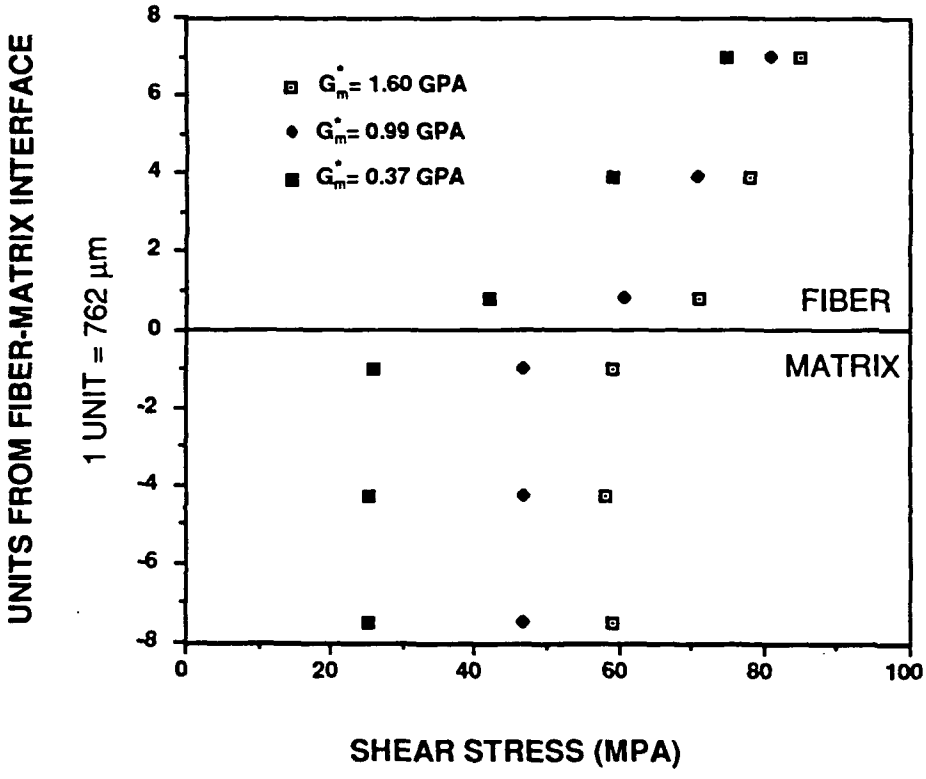

* Value of matrix shear modulus used in finite element analysis

Figure 32 Rotated Shear Stresses at the Integration Points on Either Side of the Fiber-Matrix Interface a/L = 0.009

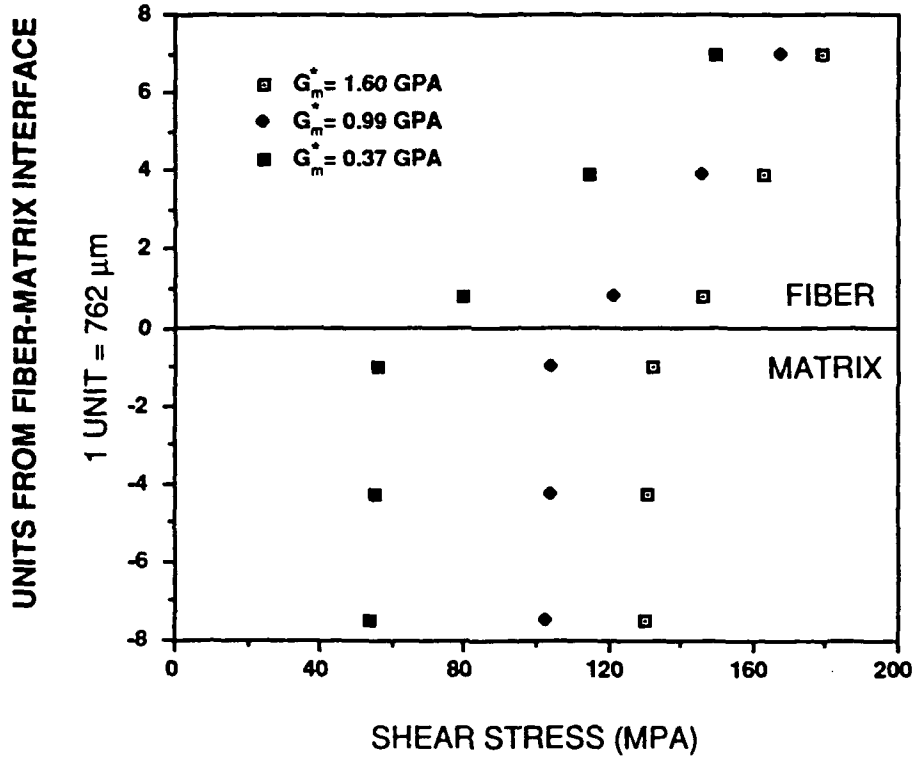

* Value of matrix shear modulus used in finite element analysis

INITITAL DISTRIBUTION

Copies

12 DTIC

5 NAVSEA
- 1 05M3 (Pinto)
- 1 92R (Swann)
- 1 92R (Spero)
- 1 55Y2 (Provencher)
- 1 55Y2 (Will)

3 NRL
- 1 6383 (Badaliance)
- 1 6383 (Wolock)
- 1 6385 (Chaskelis)

1 NSWC
- 1 R31 (Augl)

5 ONR
- 1 1132SM (Rajapakse)
- 1 1131S (Fishman)
- 1 1132SM (Barsoum)
- 1 1216 (Vasudevan)
- 1 1132SM (Jones)

1 ONT
- 1 225 (Kelly)

CENTER DISTRIBUTION

Copies	Code	Name
1	0115	Caplan
1	0113	Douglas
1	17	Krenzke
1	1702	Corrado
1	172	Rockwell
1	176	Sykes
1	1720.2	Phyillaier
1	1720.4	Wiggs
1	1730.2	Critchfield
1	2723	Wilhelmi
1	274	Wang
1	28	Wacker
1	2801	Crisci
1	2802	Morton
1	2803	Cavallaro
1	2814	Montiel
1	284	Fischer
1	2844	Castelli
5	2844	Gipple
1	522.2	TIC (A)
1	522.1	TIC (C)
1	5231	Office Services

REPORT DOCUMENTATION PAGE

Form Approved
OMB No. 0704-0188

1. AGENCY USE ONLY *(Leave blank)*	2. REPORT DATE	3. REPORT TYPE AND DATES COVERED
	October 1990	Final report – June 89 to October 90

4. TITLE AND SUBTITLE
A Comparison of the Compression Response of Thick (6.35 mm) and Thin (1.60 mm) Dry and Moisture Saturated AS4/3501–6 Laminates

5. FUNDING NUMBERS
Program Element 62234N and 61152N; Project No. ZR00001, Task No. R3450S0S, R000N00, Work Unit No. 2802–950 and 2844–220

6. AUTHOR(S)
Karin Gipple

7. PERFORMING ORGANIZATION NAME(S) AND ADDRESS(ES)
David Taylor Research Center
Bethesda, MD 20084–5000

8. PERFORMING ORGANIZATION REPORT NUMBER
DTRC–SME–90/74

9. SPONSORING /MONITORING AGENCY NAME(S) AND ADDRESS(ES)
DTRC Materials Block, IR

10. SPONSORING /MONITORING AGENCY REPORT NUMBER

11. SUPPLEMENTARY NOTES

12a. DISTRIBUTION / AVAILABILITY STATEMENT
Approved for public release, distribution is unlimited.

12b. DISTRIBUTION CODE

13. ABSTRACT *(Maximum 200 words)*

The compression response of thick (6.35 mm) and thin (1.60 mm) $(0_2/90)_s$ AS4/3501–6 laminates was compared for material in the dry and moisture saturated conditions. The thick specimens failed at 1055 MPa dry and 740 MPa wet. Comparable strengths for the thin specimens were 1090 and 957 MPa. There was no statistical difference in strength for the dry material of either thickness. The thick specimens absorbed significantly more water than the thin specimens, and consequently, showed a greater loss in compression strength.

The elastic modulus was not affected by moisture in the thick or thin specimens. The gross failure mode of the dry and wet specimens of either thickness was very similar with slightly more delamination occurring in the wet specimens. The thick specimens typically exhibited angular cracks of 27 to 30° partially across the specimen thickness. This was not observed in the thin specimens.

Finite element techniques were used to determine shear stresses in the matrix for a fiber-matrix composite plate with an initial imperfection, and loaded in compression. These matrix shear stresses were used in a compression failure theory which showed reasonable agreement with experimental results. It appears that the detrimental influence of the moisture is the degradation of the matrix shear modulus at high compressive stresses with high moisture concentrations.

14. SUBJECT TERMS
Composite materials, Compression testing of composites, Thick composites, Compression failure theories, Moisture effects on composite materials

15. NUMBER OF PAGES
110

16. PRICE CODE

17. SECURITY CLASSIFICATION OF REPORT	18. SECURITY CLASSIFICATION OF THIS PAGE	19. SECURITY CLASSIFICATION OF ABSTRACT	20. LIMITATION OF ABSTRACT
Unclassified	Unclassified	Unclassified	